

RESEARCH ARTICLE

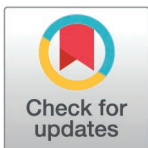
Intracellular *Pseudomonas aeruginosa* persist and evade antibiotic treatment in a wound infection model

Stéphane Pont^{1#}, Flore Nilly¹, Laurence Berry¹, Anne Bonhoure¹, Morgan A. Alford², Méli ssande Louis³, Pauline Nogaret¹, Manjeet Bains², Olivier Lesouhaitier³, Robert E. W. Hancock², Patrick Plésiat⁴, and Anne-Béatrice Blanc-Potard^{1*}

1 Laboratory of Pathogens and Host Immunity (LPHI), Université de Montpellier, CNRS, Inserm, 34095, Montpellier, France, **2** Center for Microbial Diseases and Immunity Research, University of British Columbia, Vancouver, Canada, **3** CBSA UR4312, Laboratoire de microbiologie Communication Bactérienne et Stratégies Anti-Infectieuses, Univ Rouen Normandie, Université Caen Normandie, Normandie Univ, Rouen, France, **4** UMR6249 CNRS Chrono-environnement, Université de Franche-Comté, Besançon, France

Present address: Centre International de Recherche en Infectiologie (CIRI), Université de Lyon, Inserm U1111, Université Claude Bernard Lyon 1, CNRS UMR5308, ENS de Lyon, Lyon, France

* anne.blanc-potard@umontpellier.fr



OPEN ACCESS

Citation: Pont S, Nilly F, Berry L, Bonhoure A, Alford MA, Louis M, et al. (2025) Intracellular *Pseudomonas aeruginosa* persist and evade antibiotic treatment in a wound infection model. PLoS Pathog 21(2): e1012922. <https://doi.org/10.1371/journal.ppat.1012922>

Editor: Vincent T Lee, University of Maryland, UNITED STATES OF AMERICA

Received: July 3, 2024

Accepted: January 22, 2025

Published: February 13, 2025

Copyright: © 2025 Pont et al. This is an open access article distributed under the terms of the [Creative Commons Attribution License](https://creativecommons.org/licenses/by/4.0/), which permits unrestricted use, distribution, and reproduction in any medium, provided the original author and source are credited.

Data availability statement: All data needed to evaluate the conclusions of this study are presented in the paper and/or the Supplementary Materials. Further information for resources and reagents should be directed to and will be fulfilled by A.B.B.P. at LPHI, CNRS, France (anne.blanc-potard@umontpellier.fr). Our submission contains all raw data required to replicate the results of your study.

Abstract

Persistent bacterial infections evade host immunity and resist antibiotic treatments through various mechanisms that are difficult to evaluate in a living host. *Pseudomonas aeruginosa* is a main cause of chronic infections in patients with cystic fibrosis (CF) and wounds. Here, by immersing wounded zebrafish embryos in a suspension of *P. aeruginosa* isolates from CF patients, we established a model of persistent infection that mimics a murine chronic skin infection model. Live and electron microscopy revealed persisting aggregated *P. aeruginosa* inside zebrafish cells, including macrophages, at unprecedented resolution. Persistent *P. aeruginosa* exhibited adaptive resistance to several antibiotics, host cell permeable drugs being the most efficient. Moreover, persistent bacteria could be partly re-sensitized to antibiotics upon addition of anti-biofilm molecules that dispersed the bacterial aggregates *in vivo*. Collectively, this study demonstrates that an intracellular location protects persistent *P. aeruginosa in vivo* in wounded zebrafish embryos from host innate immunity and antibiotics, and provides new insights into efficient treatments against chronic infections.

Author summary

Chronic bacterial infections represent a major clinical issue due to their ability to escape the immune system and antibiotic treatments and our work provides major advances to track and tackle persistent bacterial infection in a living host. Using a zebrafish model of infection with *Pseudomonas aeruginosa* clinical isolates from cystic fibrosis patients, our study reveals the contribution of intracellular *P. aeruginosa* to bacterial persistence *in vivo*, which is associated with protection from clearance by host and antibiotics. Conversely, our findings underline the importance of strategies efficiently targeting the

Funding: Work in ABBP's team was supported by Vaincre La Mucoviscidose (<https://www.vaincrelamuco.org/>)(RF20200502703, RIF20210502864, RF20220503060) and Association Gregory Lemarchal. REWH was supported by Canadian Institutes for Health Research grant FDN-154287 as well as a UBC Killam Professorship. The funders played no role in the study design, data collection and analysis, decision to publish, or preparation of the manuscript.

Competing interests: The authors have declared that no competing interests exist.

protective intracellular niche of *P. aeruginosa* and show unprecedented opportunities provided by the zebrafish model for drug testing in the context of persistent infection.

Introduction

Many bacterial pathogens can persist inside their hosts for long periods of time, due to immunodeficiency of the host, immune evasion by the bacteria and/or ineffective antibiotic treatments. *Pseudomonas aeruginosa* is a Gram-negative bacterium ubiquitous in watery environments and a major cause of a variety of nosocomial infections worldwide [1], including urinary tract, respiratory tract, wound/skin and blood infections. *P. aeruginosa* infections can be either acute or chronic, implying different virulence strategies to evade host immunity [1]. Chronic colonization is frequent during cystic fibrosis (CF), non-CF bronchiectasis or chronic obstructive pulmonary disease (COPD), and also occurs on wounds [2,3]. In long-lasting lung infections in CF patients, *P. aeruginosa* adopts a sessile lifestyle, with bacterial communities organized in a biofilm structure, impeding bacterial clearance by the immune system [4].

P. aeruginosa, which is well known for its capacity to develop resistance to antibiotic treatments, belongs to the threatening group of ESKAPEE pathogens, and was recognized by the World Health Organization as a critical priority for new therapeutics in 2017 [5] and high priority in 2024. Chronic bacterial infections are challenging to treat with antibiotics due to a combination of intrinsic, acquired, and adaptive drug resistance, along with the specific bacterial lifestyle in infected tissues. The adaptive resistance to antibiotics, which is a phenotypic non-heritable trait [6], is related to several factors, including biofilm lifestyle, slow growth and low metabolic activity [7]. Moreover, increasing evidence supports the idea that *P. aeruginosa* undergoes an intracellular life cycle during infection [8,9], including human pulmonary infection as shown with the recent observation of intracellular *P. aeruginosa* in the airway epithelium of CF lung explants [10]. Whereas intracellular localization was shown to affect drug efficacy against *P. aeruginosa* in cell culture models [11–13], this aspect has not been addressed *in vivo*, especially in the context of a persistent infection.

While a plethora of *in vivo* models have been used to assess *P. aeruginosa* virulence, only a small subset were aimed at studying this pathogen in the context of persistent colonization and testing the efficacy of treatments on chronic infection [14]. Current animal models to study *P. aeruginosa* respiratory chronic pathogenesis mainly rely on lung administration of bacteria embedded in agar/agarose beads [15]. A murine chronic skin infection model has also been developed, mimicking long-term colonization in humans [16]. Zebrafish (*Danio rerio*), a vertebrate that shows the advantages of invertebrates (moderate ethical issues, low cost, high production of eggs), represents an appealing *in vivo* model for drug testing and high-resolution real-time visualization of *P. aeruginosa* and host cells due to embryo transparency [17]. More specifically, the zebrafish innate immune system is very similar to that of mammals, notably regarding phagocytic cells (neutrophils and macrophages) and soluble immune mediators such as cytokines and complement proteins [18]. Real time *in vivo* imaging has previously allowed the visualization of the interaction of *P. aeruginosa* with innate immune cells in the context of acute infections [17,19,20].

In this study, we established a model of persistent colonization of the zebrafish embryo by *P. aeruginosa*, using a caudal wound infection protocol and *P. aeruginosa* CF clinical isolates. The visualization of persisting bacteria revealed the importance of an intracellular phase, notably inside macrophages, and the formation of bacterial aggregates *in vivo*. Persistent bacteria became less responsive to treatment by several classes of antibiotics, and host cell permeable antibiotics were found to be more efficient. In addition, antibiotic efficacy against persistent bacteria could be potentiated by addition of anti-biofilm compounds. This work offers an *in vivo* model to investigate the contribution of intracellular *P. aeruginosa* to chronic

infection, with unprecedented imaging capabilities, and paves the way to assess the efficacy of therapeutics in the context of a persistent colonization.

Results

Zebrafish embryo is an appropriate model to monitor a persistent infection with *P. aeruginosa* CF isolates

While reference laboratory strains causing acute infections (PAO1, PA14, and PAK) have been widely used in the zebrafish model to gain insights into the host-*P. aeruginosa* interaction *in vivo*, investigations of the pathogenesis of clinical isolates in this vertebrate model have remained very scarce, and relied on the microinjection of single CF isolates [21,22]. We recently developed a wound infection protocol in zebrafish based on the immersion of tail fin-amputated embryos with *P. aeruginosa* PAO1 strain, which caused an acute infection within 20 hours post infection (hpi) [23]. The immersion of injured embryos is a mode of infection that is easier than microinjection, reproducible, amenable to confocal and electron microscopy and reflecting a natural infection by *P. aeruginosa*. Here, we used this infection mode to evaluate the *in vivo* virulence of three CF isolates (A6520, B6513 and C6490), that were not tested earlier for virulence or persistence in any infection model. Genome sequencing indicated that these three strains, all positive for *exoS* gene, belong to distinct serotypes (ST274, ST27 and ST633). The survival of zebrafish embryos was first monitored over 40 hpi (Fig 1A). All three CF isolates were highly attenuated, being associated with 90% (A6520, B6513) to 100% (C6490) survival, when compared to the reference strain PAO1 (50% survival) (Fig 1B). Additional experiments were next conducted on these CF isolates to assess whether their attenuated phenotype was linked to the elimination or not of the bacteria by the host.

To discriminate between bacterial clearance and bacterial persistence, we assessed the evolution of the bacterial load per embryo over 72 hpi. To easily recognize and count *P. aeruginosa* bacteria, we used green-fluorescent strains harboring a chromosomally-integrated *gfp* gene with constitutive expression, to avoid the risk of GFP signal loss upon time. For all strains, a notable variability between individual larvae was noticed, with some differences being > 100-fold ($2 \log_{10}$), but the distribution profiles were reproducible between independent experiments. In surviving embryos infected with the reference strain PAO1, a continuous decrease of bacterial load was found over time but some bacteria were persisting (Fig 1C), which is consistent with a previous study using a different infection mode [24]. With isolates A6520 and C6490, the majority of the embryos were observed to be free of bacteria at 67 or 43 hpi, respectively (Fig 1C). Conversely, with strain B6513, 90% of the bacteria were eliminated between 1.5 to 18 hpi, but the remaining bacterial load (median of 630 CFU) stayed relatively constant in numbers until 65 hpi (Fig 1C). Thus, isolate B6513 developed a persistent infection in this immersion zebrafish model, whereby a subset of bacteria survived after 18 hpi without killing the host. The residual CFU analysis for isolate B6513 was extended up to 6 days post-infection (dpi) and an increased number of persistent bacteria per fish was observed compared to 3 dpi. However, further studies would be required at 6 dpi to differentiate the persistent bacteria from possible reinfections through mouth ingestion. Subsequent experiments were carried out only on embryos for up to 3 dpi (i.e., 5 days post-fertilization, within the frame not regulated as animal experiments) to follow the 3R-principle and limit a possible reinfection upon food ingestion.

To extend the relevance of this model, we assessed the virulence and persistence of the well characterized isolate RP73, a late CF isolate capable of long-term colonization in mouse airways [25,26]. Consistent with previous mouse studies, and similarly to strain B6513, the RP73 isolate failed to induce embryo mortality and persisted in infected zebrafish embryos

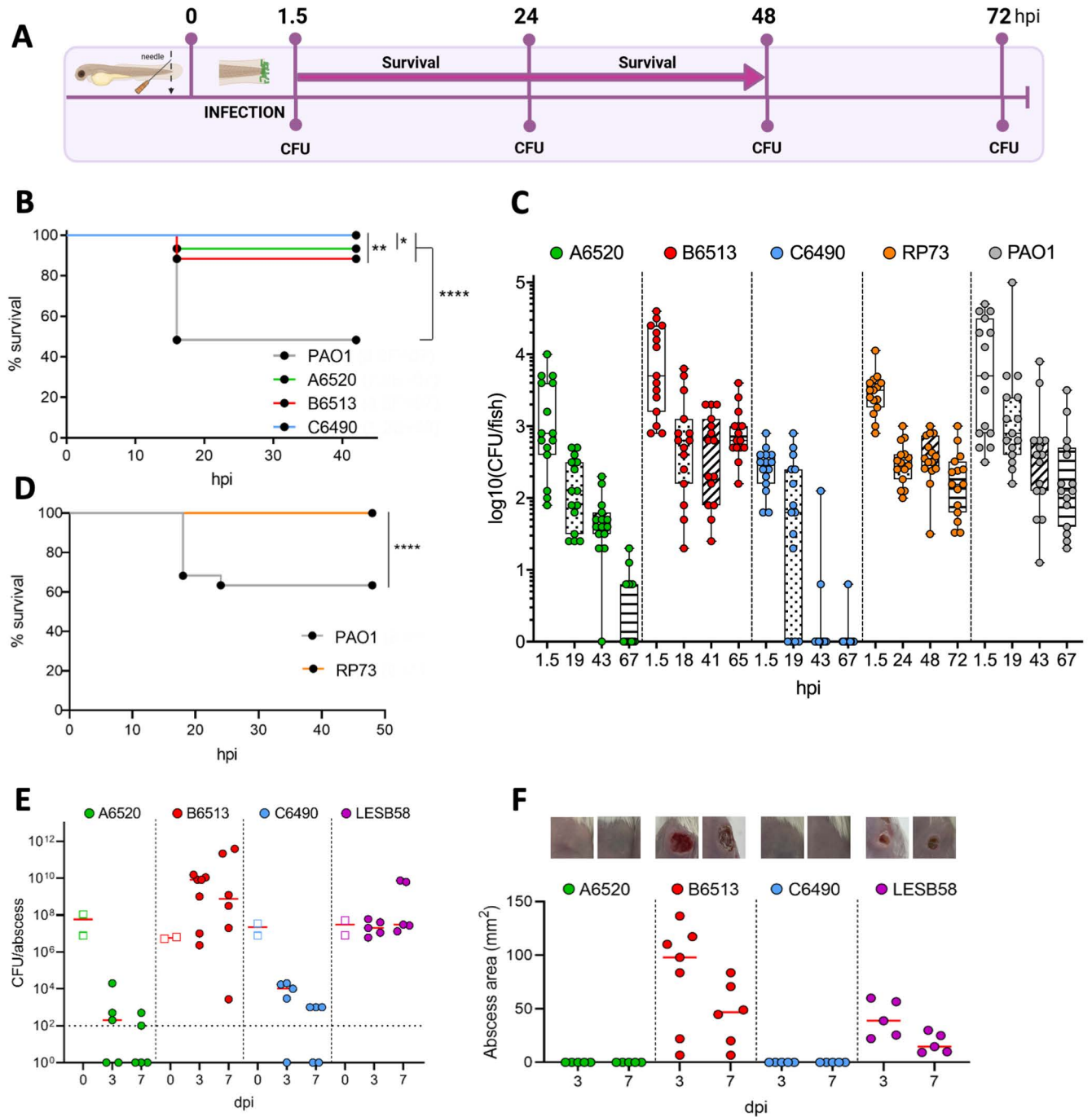


Fig 1. CF isolates can establish a persistent infection in zebrafish embryos, with parallel profiles to a murine model of infection. (A) Experimental timeline to assess bacterial virulence and persistence in zebrafish embryo. Drawing was created with BioRender.com. (B) and (D) Embryo survival following infection by immersion with indicated *P. aeruginosa* strains at bacterial concentrations ranging from 7.2×10^7 to 1.2×10^8 CFU/mL. Survival was monitored for > 40h following the infection (n = 3, 60 larvae in total). Log-rank test: * $P < 0.05$, ** $P < 0.01$ and **** $P < 0.0001$. (C) Evolution of the bacterial load per embryo over time (until 72 hpi). Following infection by immersion with GFP⁺ *P. aeruginosa* isolates, embryos were crushed at the indicated time points and plated for CFU counting (n = 3, 15 larvae). (E) and (F) Virulence and persistence of CF isolates in a murine model of high-density cutaneous infection. Bacterial load (E) and size of abscesses (F) formed for three or seven days in CD-1 mice subcutaneously injected with indicated *P. aeruginosa* strains in the right dorsum were quantified. The CFUs reported at 0 dpi (empty squares) correspond to the injected inoculum. At 3 dpi and 7 dpi, abscesses were measured and harvested in phosphate buffered saline (PBS), homogenized and plated on lysogeny broth (LB) for bacterial enumeration. Data from two independent experiments containing 2–4 biological replicates each (n = 5–7) are displayed as the median. The limit of detection (LOD) is displayed as a dashed line at 10^2 CFU/abscess. The photo insets above the graph are representative images from treatment groups (M.A.A is the photographer).

<https://doi.org/10.1371/journal.ppat.1012922.g001>

(Fig 1C and 1D). To verify that the persistent phenotype reflected colonization of the wound and not the ability of the isolates to adhere to the embryo's skin, we assessed the bacterial load over time in uninjured embryos incubated with persistent strains B6513 and RP73. At 24 hpi, no CFU were detected for either isolate (S1 Fig), showing that the injury was required to drive a persistent infection.

We next addressed the behaviour of the three CF isolates A6520, B6513 and C6490 in a mouse model of chronic infection that involves cutaneous abscesses [16]. *P. aeruginosa* LESB58, a well-characterized CF isolate that causes chronic lung infection and chronic skin abscess in mice [16,27], was used as a reference to assess *in vivo* growth and virulence of the clinical isolates over a seven-day period after subcutaneous injection in mice (with approx. 5×10^7 CFU). As previously reported, *P. aeruginosa* LESB58 persisted at the infection site, being recovered at median densities above 10^7 CFU/abscess at 3 and 7 dpi (Fig 1E). Similarly, the clinical isolate *P. aeruginosa* B6513 was recovered at high median densities, $> 10^8$ CFU/abscess at 3 and 7 dpi. In contrast, clinical isolates *P. aeruginosa* A6520 and C6490 were mostly eliminated from the host when compared to the other strains, as reflected by low median bacterial densities ($< 10^4$ CFU/abscess at 3 dpi, and 10^3 or below the limit of detection at 7 dpi). Trends in abscess sizes were reflective of bacterial recovery from the localized infection site at both time points, with abscess (dermonecrotic cutaneous tissue) lesion areas of 15–39 mm² and 47–98 mm² for strains LESB58 and B6513, respectively, whereas strains A6520 and C6490 did not cause abscess formation (Fig 1F). Healing of the cutaneous tissue appeared to occur at 7 dpi for both *P. aeruginosa* LESB58 and B6513, since the sizes of abscesses had decreased (–24 and –51 mm² respectively) relative to the abscesses of animals sacrificed 3 dpi. Accordingly, the mean clinical scores of animals decreased during the time from 3 to 7 dpi across treatment groups (S2 Fig). Furthermore, clinical scores of animals remained low overall, with a maximum recorded total score of 8/50 (in the *P. aeruginosa* B6513 treatment group), indicating that none of the strains caused severe disease in animals.

Taken together, our results showed that the injured embryo immersion model of zebrafish infection is suitable to assess persistence of *P. aeruginosa* clinical isolates. Importantly, the persistence profiles of strains in zebrafish are consistent with the phenotypes observed in a murine chronic infection model. We next took advantage of the unique imaging opportunities offered by the zebrafish embryo to visualize persisting bacteria at high resolution.

Dynamic interaction of persistent *P. aeruginosa* with host immune cells *in vivo*

Macrophages and neutrophils have been shown to rapidly phagocytose *P. aeruginosa* upon zebrafish infection [20,28–30]. We took advantage of the optical transparency of embryos to image GFP-expressing isolate B6513 throughout the infection, assess bacterial morphology, localization and interaction with recruited macrophages, using Tg(*mfap4::mCherry-F*) zebrafish embryos that harbor red fluorescent macrophages. Consistent with CFU counts, we observed a decrease in the GFP⁺ bacteria between 1.5 and 24 hpi (Fig 2A). At 1.5 hpi, most bacteria appeared outside of mCherry labeled macrophages, while at 24 and 65 hpi, they mainly appeared as foci localized nearby the injury site (Fig 2A). Intra-macrophagic *P. aeruginosa* were present throughout the course of infection (Fig 2A) and a 3D reconstruction is shown in Fig 2B (the sequential Z stack slices of the 3D reconstruction are shown in S3 Fig). The presence of bacterial foci, with putative localization inside macrophages, was not specific to the B6513 isolate since similar findings were visualized with the RP73 strain (S4 Fig). The rare persistent bacteria visualized with PAO1 strain can also be found inside macrophages (S4 Fig), as reported earlier using a different infection mode [24]. Bacterial aggregates were retained within macrophages for 10 h or more, as shown using time-lapse confocal

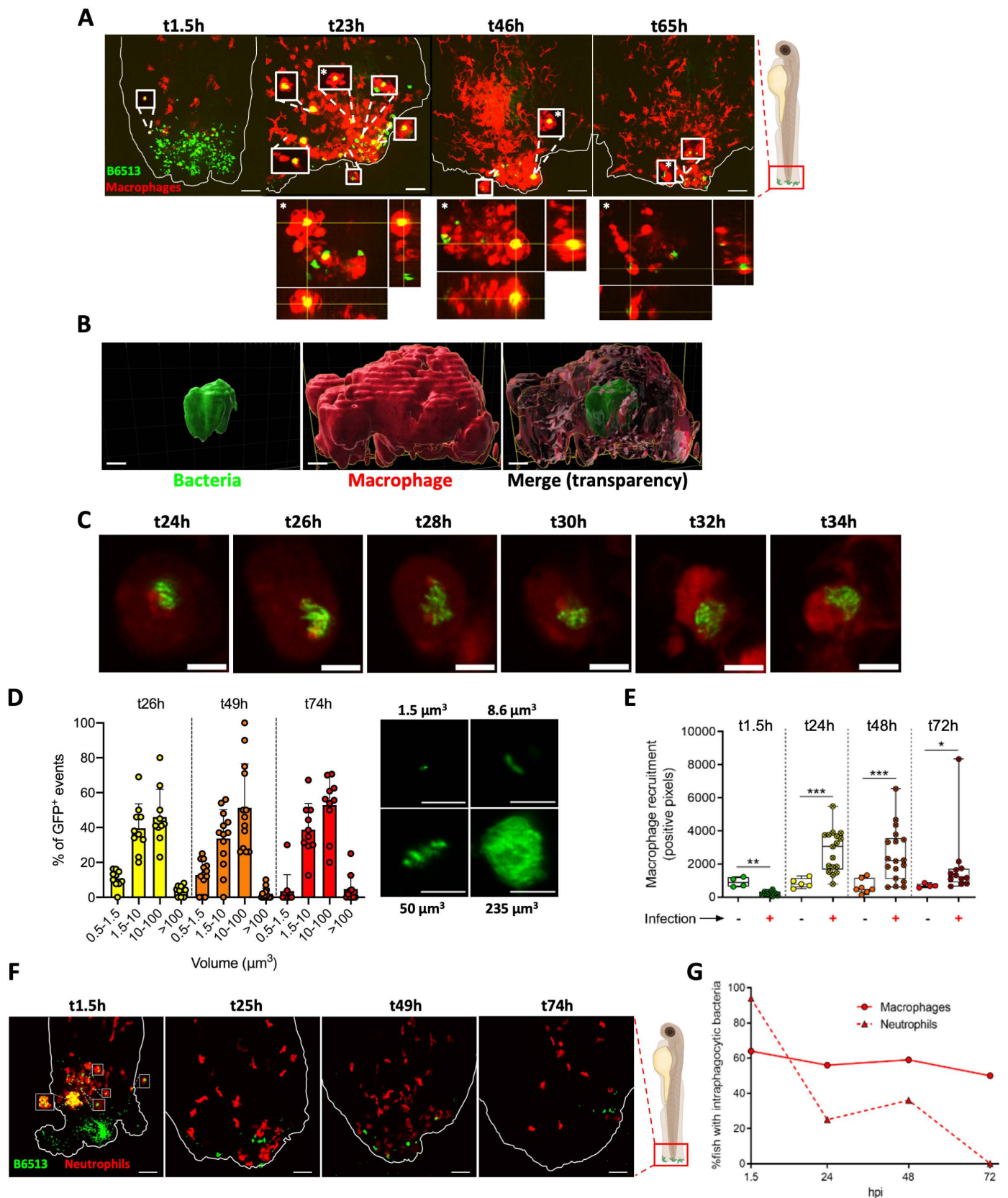


Fig 2. Upon persistent colonization, *P. aeruginosa* B6513 forms aggregates which can be visualized inside macrophages but not neutrophils. (A) Representative maximal projections of confocal images, showing interactions between bacteria (green) and recruited macrophages (red) in Tg(*mfp4:mCherry-F*) larvae at different

time points. White rectangles denote images extracted from a single optical section of macrophages with intracellular *P. aeruginosa*. Below the images, orthogonal representations of the (*) events are shown, confirming that bacteria were inside macrophages (only one example of orthogonal view is shown but intracellular location applies to all rectangles). Scale bar: 40 μm . Note that pictures come from different embryos imaged for each indicated times (10 to 17 larvae at each time point). (B) 3D reconstruction allowing to confirm the intra-macrophagic localization of a bacterial foci. Scale bar: 7 μm . (C) Zoomed single optical sections of an intra-macrophagic bacterial aggregate tracked from 24 hpi to 34 hpi using time-lapse confocal imaging. Image acquisition was done every 30 min and images corresponding to 2 h intervals are shown. Brightness/contrast settings were modified comparatively to (A) for a better visualization of the aggregate organization after a deconvolution. Scale bar: 5 μm . (D) Volume repartition of total GFP⁺ events per larvae quantified following 3D reconstruction (10 to 13 embryos were imaged at each time point), along with representative images (single Z-plans) of the four types of size clusters for GFP⁺ events. (E) Macrophage quantification at the wound, measured by the number of red pixels at the median plan of the stack, in presence or absence of bacteria at various time points (4 to 8 control and 8 to 18 infected embryos were imaged at each time point). Mann-Whitney test: * $P < 0.05$, ** $P < 0.01$ and *** $P < 0.001$. (F) Representative maximal projections of confocal images, showing interactions between bacteria (green) and recruited neutrophils (red) in Tg(*LysC:dsRed*) larvae. White rectangles denote images extracted from a single optical section of neutrophils with intracellular *P. aeruginosa*. Scale bar: 40 μm . Note that pictures come from different embryos imaged for each indicated times (12 to 16 larvae at each time point). (G) Evolution of the proportion of Tg(*mfp4:mCherry-F*) and Tg(*LysC:dsRed*) larvae with at least one event of intra-macrophage or intra-neutrophil bacteria, respectively, over time (10 to 16 larvae were imaged at each time point). Only colonized embryos (presence of GFP⁺ events) with detectable macrophages or neutrophils (mCherry⁺ signal) were included in the analysis. Drawings in panels A and F were created with BioRender.com.

<https://doi.org/10.1371/journal.ppat.1012922.g002>

microscopy (Fig 2C). The size distribution of GFP positive spots was stable over time, with a volume mainly comprised between 1.5 μm^3 (individual bacteria) and 100 μm^3 (clusters) in size (Fig 2D). Larger foci (> 100 μm^3) were observed in some embryos. Infection seemed to delay macrophage recruitment to the wound at the early time point (1.5 hpi, Fig 2E). Macrophage recruitment in infected embryos peaked at 24 hpi and decreased slowly, being close to the level of uninfected controls at 72 hpi (Figs 2E and S5).

The interaction of persistent bacteria with neutrophils using the Tg(*LysC:dsRed*) transgenic line harboring red fluorescent neutrophils was subsequently investigated (S6 Fig). In agreement with previous experiments done on microinjected embryos [28–30], numerous intra-neutrophilic *P. aeruginosa* were observed shortly after colonization (Fig 2F and 2G). However, this frequency was strongly reduced at 24 and 48 hpi (S6 Fig), and no intra-neutrophil bacteria were observed at 72 hpi. On the other hand, the association between *P. aeruginosa* and macrophages was maintained over time with around 60% of infected embryos having at least one event of intra-macrophage bacteria (Fig 2G), whereas the remaining infected embryos displayed no intra-macrophage bacteria (S4 Fig). In embryos with at least one intra-macrophage event, the percentage of GFP⁺ foci inside macrophages was around 14%, 32% and 34% at 24, 48 and 72 hpi, respectively (high bacterial load at 1.5 h precluded image quantification of the GFP signal, but GFP⁺ foci inside macrophages were estimated below 3% at this early time point). Thus, the kinetics of appearance of intra-neutrophil and intra-macrophage bacteria were very different (Fig 2G), suggesting that the interaction with neutrophils was restricted to the early steps of colonization and/or that the killing activity of neutrophils and/or their short half-life prevented any intra-neutrophilic persistence of *P. aeruginosa*. Cumulatively, this live imaging analysis revealed transition from bacteria mostly outside macrophages and neutrophils to persistent clusters in an intra-macrophage niche.

High resolution imaging of the intracellular niche of persistent bacteria

As described above, live imaging revealed the presence of persistent *P. aeruginosa* bacteria, both inside and outside macrophages at 24 and 48 hpi (Fig 2A and 2G), but likely not within neutrophils (Fig 2F and 2G). Since *P. aeruginosa* can also enter and reside within non-phagocytic cells [31–33], we investigated their presence within non-phagocytic cells at the infection site. To this aim, we used Tg(*rcn3:Gal4/UAS:mCherry*) transgenic embryo harboring red fluorescent mesenchymal cells. Intracellular bacteria (individual or clusters) were clearly visualized at 24 and 48 hpi (S7 Fig), demonstrating that *P. aeruginosa* also uses this niche *in vivo*, supporting pioneer work carried out with mice corneal infections [9,33].

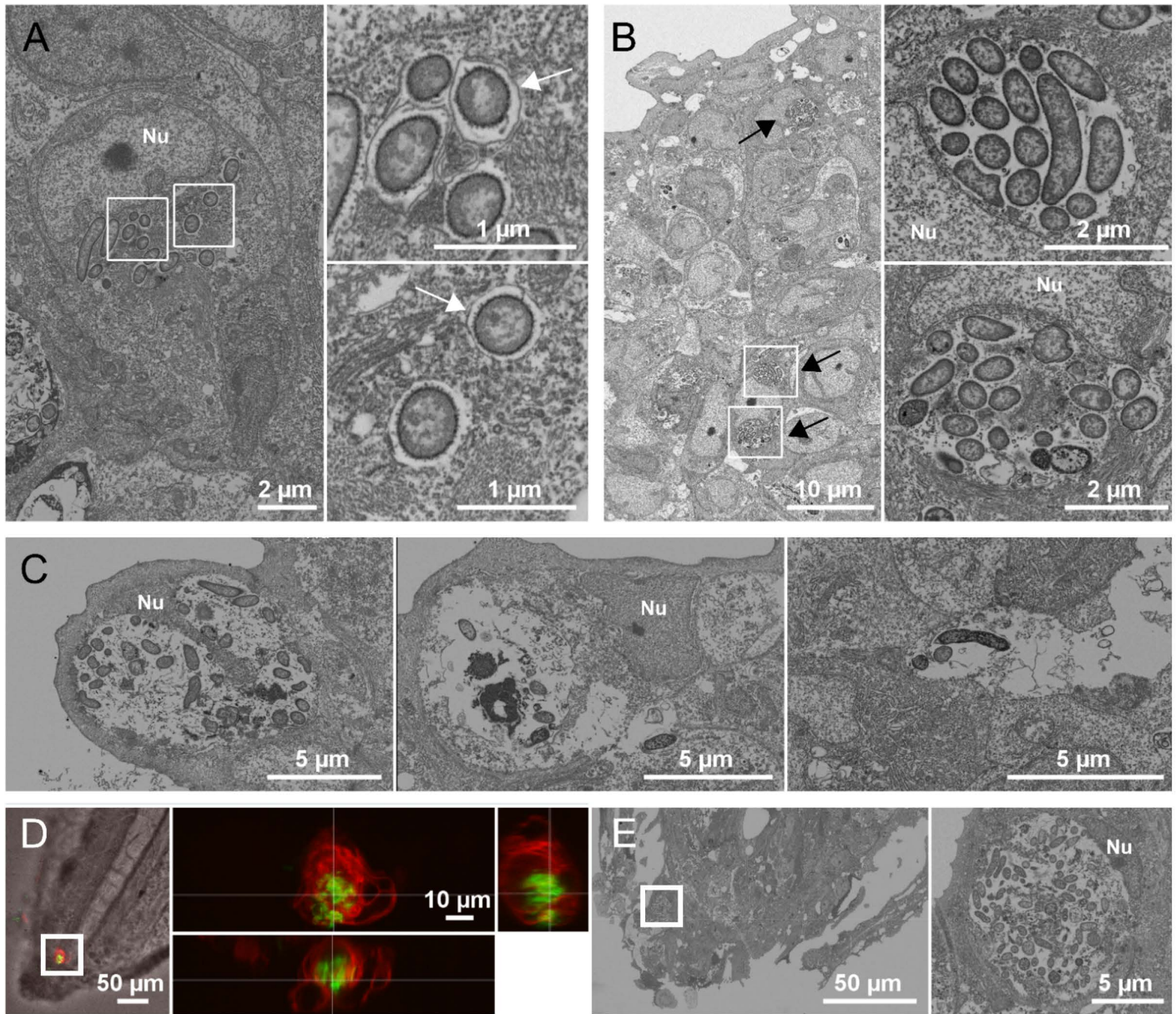


Fig 3. Electron micrographs of persistent *P. aeruginosa* B6513 in zebrafish. Representative images were acquired from serial thin sections of infected embryos at 24 hpi (D-E) or 48 hpi (A-C). (A) High magnification images of single intracellular bacteria near the tail fin edge (pixel size 5 nm). Right panels show enlargements of the white squares. Nu: cell nucleus. A membrane is visualized around some bacteria (white arrow). (B) Overview of the tail fin region (pixel size 20 nm) showing clustered intracellular bacteria in a vacuolar-like shape (black arrows). Right panels show higher magnification (pixel size 5 nm) of the white squares. (C) High magnification images of intracellular bacteria in highly damaged cell (left panel) or in necrotic cell ghost (middle panel), or of bacteria in the extracellular space (right panel). (D) and (E) Correlative Light-electron Microscopy (CLEM). (D) A z-stack of a live zebrafish embryo was acquired. The left panel shows a single fluorescent plane overlaid with the central DIC image of the fish tail (macrophages are seen in red and bacteria in green). A single large cluster containing dozens bacteria inside a macrophage is shown (white square). The right panel shows the orthogonal projection of the portion of the stack containing the cluster. (E) After processing the same fish for EM, serial thin sections were prepared and imaged by EM. One section was acquired at a pixel size of 25 nm. Left panel shows an overview of the tail region. The large cluster observed in panel D in light microscopy is shown in its physiological context in the left panel (white square). The portion of the image containing the cluster is enlarged on the right panel, showing a high number of bacteria, filling almost all the cytoplasm of the cell and leaving the nucleus intact on one side.

<https://doi.org/10.1371/journal.ppat.1012922.g003>

We used electron microscopy (EM) to highlight the ultrastructural context of persistent bacteria in the tail fin of 24 or 48 hpi fixed infected Tg(*mfap4::mCherry-F*) embryos (Fig 3). Bacteria were largely seen inside cells, either single (Fig 3A) or in clusters (Fig 3B). A detailed analysis indicated that some bacteria were rather localized in vacuoles, as shown by the shape of clusters and/or the visualization of a vacuolar membrane, whereas other appeared free in the cytoplasm (Fig 3A). Some cells with intracellular bacterial cluster appeared highly damaged (Fig 3C, left panel) and bacteria could be seen in cell remnants, containing a nucleus but essentially devoid of cytoplasm, suggesting necrotic cells (Fig 3C, middle panel). Rare bacteria could be visualized in the extracellular space (Fig 3C, right panel). Since identifying the host-cell type only by ultrastructural criteria was challenging, we also performed correlative Light-Electron Microscopy (CLEM) (Fig 3D and 3E). A single large cluster of bacteria inside a macrophage was found by light microscopy (Fig 3D). The same embryo was processed for EM and serial sections were prepared and imaged by array tomography (Fig 3E). The same cluster, highlighted by a white square in panels D and E, showed a high number of bacteria inside a cell identified as a macrophage by the corresponding fluorescence image.

Taken together, live and electron microscopy analyses indicated that *P. aeruginosa* bacteria persisting at the infection site were largely intracellular, in either macrophages or non-phagocytic cells. Moreover, CLEM imaging allowed visualization of a large cluster of *P. aeruginosa* inside a macrophage. These findings support the uniqueness of the zebrafish model in deciphering how *P. aeruginosa* interacts with host cells during infection.

Strains with a persistent profile in zebrafish survived inside cultured macrophages and formed biofilms *in vitro*

In our *in vivo* model, persistent *P. aeruginosa* were visualized as intra-macrophage bacterial clusters at the zebrafish wound site (Figs 2 and 3). We addressed the *in vitro* features of the CF isolates by investigating their phenotypes in a macrophage cell line and in a biofilm assay. We first monitored the intra-macrophagic survival of the different clinical strains by performing a gentamicin protection assay in murine J774 cells infected at a multiplicity of infection (MOI) of 10, as done previously with PAO1 [34,35]. After 1.5 h of internalization, quantification of intracellular bacteria revealed that strain A6520 was largely eliminated, while the number of C6490 and RP73 cells were only modestly reduced (Fig 4A). On the other hand, B6513 was not eliminated and survived inside macrophages for at least 1.5 h after phagocytosis (Fig 4A). Phagocytic rates of the different strains were not significantly different (Fig 4B). Time-lapse microscopy performed during 3 h after phagocytosis correlated with CFU measurements, with a striking clearance of strain A6520, not due to a disappearance of macrophages, while B6513 was still residing within macrophages (Fig 4C). The visualization of intra-vacuolar clusters with B6513 showed that this bacterium can reside in closed compartments within phagocytic cells (Fig 4D). We also assessed the cytotoxicity driven by intracellular *P. aeruginosa* strains 1.5 h after phagocytosis using Trypan blue [34]. CF isolates exhibited low or no cytotoxicity (6% dying cells for B6513 and below 1% for RP73, A6520 and C6490, versus 12% for the reference strain PAO1). We next evaluated the ability of the diverse strains to form biofilms. While A6520, B6513 and RP73 produced a pellicle covering the broth medium, C6490 failed to form such a biofilm at the air-liquid interface (Fig 4E). Moreover, we compared the swarming motility and pyocyanin production of A6520, B6513 and C6490 CF strains in comparison with PAO1 (non-CF strain) and LESB58 (CF strain). A6520, B6513 and C6490 strains exhibited no or strongly reduced swarming motility and low to mild pyocyanin production (S8 Fig).

Overall, these data show that the two isolates recognized as persistent in the zebrafish embryo model (B6513 and RP73) combined the ability to resist killing by macrophages upon

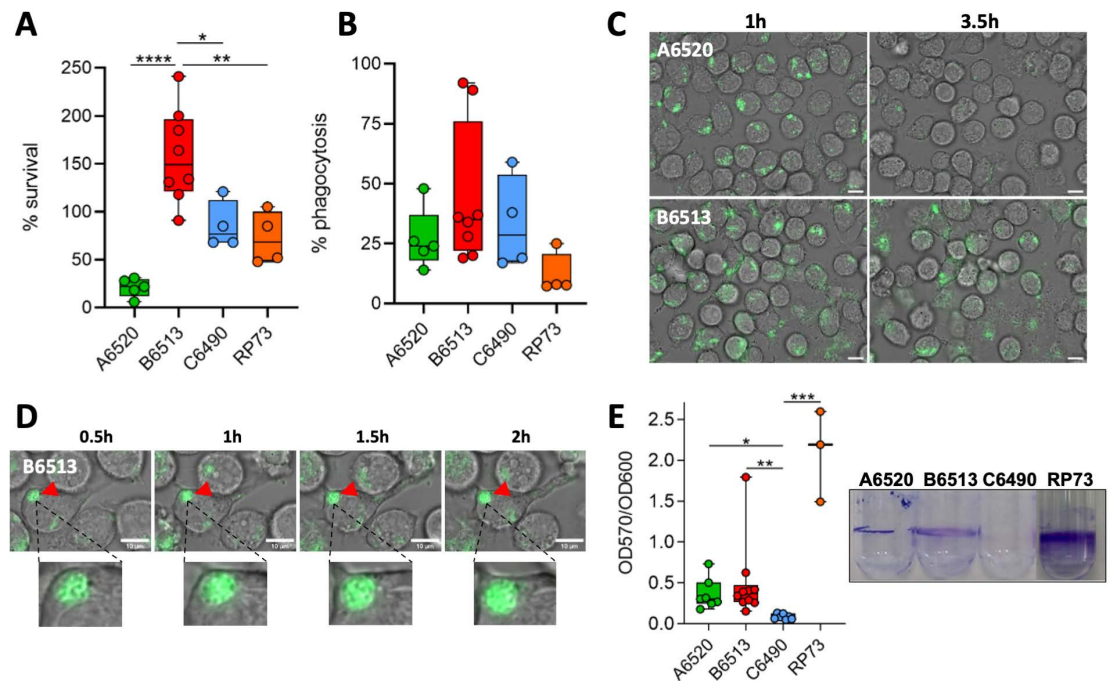


Fig 4. Persistent isolates are able to survive inside macrophages and form biofilm *in vitro*. (A) Bacterial survival within J774 macrophages ($n = 4$ to 8). The number of intramacrophagic bacteria was determined 20 min (T0) or 2 h after gentamycin treatment (T1). Survival is expressed as the ratio between the numbers of bacteria recovered at T1 versus T0. One-way ANOVA: **** $P < 0.0001$; Tukey post-hoc test: * $P < 0.05$, ** $P < 0.01$ and **** $P < 0.0001$. (B) Phagocytosis efficiency of each strain ($n = 4$ to 8). The number of intracellular bacteria recovered at T0 was compared to the initial inoculum. (C) Representative initial and final images of time-lapse microscopy to follow the behavior of GFP⁺ intramacrophagic bacteria (isolates A6520 and B6513) for 2h30. Scale bar: 10 μm . (D) Time lapse imaging of an intra-vacuolar bacterial cluster (red arrowhead) visualized within a macrophage (a zoom is shown below). In (C) and (D), times after the start of gentamycin treatment are indicated. (E) Biofilm formation at 24h assessed by crystal violet (CV) assay on glass tubes ($n = 3$ to 10). Quantification of the CV-labelled biofilm rings (a representative picture is shown on the right) is normalized with bacterial growth (OD_{600nm}). Kruskal-Wallis test: **** $P < 0.001$; Dunn post-hoc test: * $P < 0.05$, ** $P < 0.01$ and *** $P < 0.001$.

<https://doi.org/10.1371/journal.ppat.1012922.g004>

phagocytosis and the ability to form biofilms, whereas the two non-persistent isolates lacked one of these two traits. In addition, it shows that the B6513 strain, isolated from a transient infection of a one year old child, shares several features of CF-adapted isolates (low virulence, ability to form biofilm, moderate pyocyanin production and strongly reduced swarming motility). Moreover, the serotype of B6513 (ST27) has been reported at high levels in CF patients [36]. In further studies, it will be of interest to determine how the B6513 genome and transcriptome are related to those of CF-adapted strains.

Persistent *P. aeruginosa* bacteria exhibit adaptive resistance to antibiotic treatment

Antibiotic adaptive resistance is a major issue in the treatment of chronic infections. We investigated antibiotic efficacy on embryos infected by the isolate B6513, by applying a 30 min treatment at 1.5, 24 and 48 hpi (Fig 5A). Three clinically-used antibiotics to fight *P. aeruginosa* infections were tested, namely tobramycin (an aminoglycoside), colistin (a polymyxin) and ciprofloxacin (a fluoroquinolone) [37]. The minimum inhibitory concentration (MIC) of tobramycin, colistin and ciprofloxacin for B6513 was determined experimentally to be 1 $\mu\text{g}/\text{mL}$, 4 $\mu\text{g}/\text{mL}$ and 0.5 $\mu\text{g}/\text{mL}$, respectively. Antibiotics were used at 40 times the MIC (40

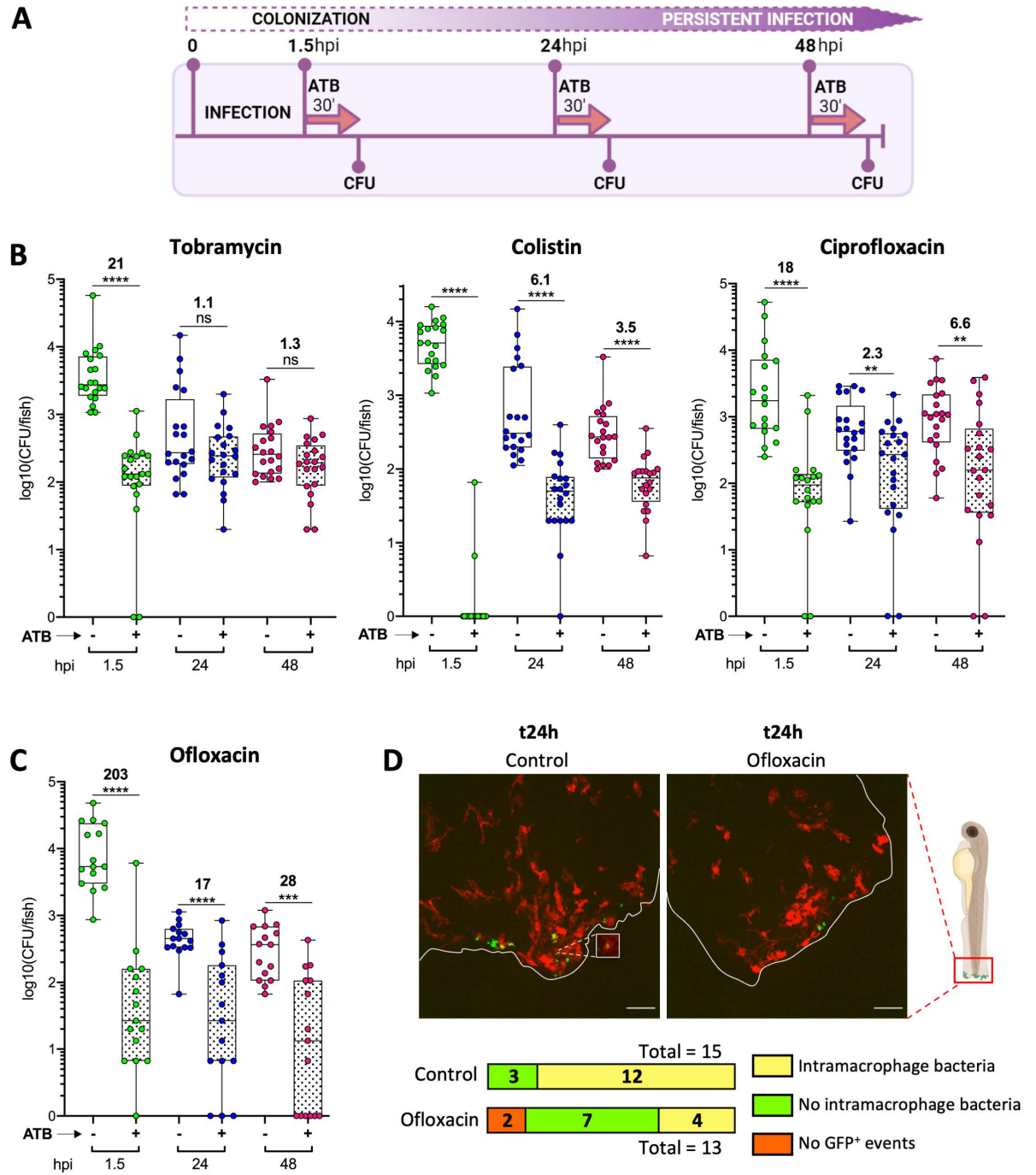


Fig 5. Antibiotics have a reduced efficacy on persistent *P. aeruginosa* in infected zebrafish. (A) Experimental procedure used to assess the efficacy of antibiotic treatments on infected embryos. ATB 30': antibiotic treatment for 30 min. (B) Efficacy of various antibiotics on strain B6513 with respect to the time post-infection (n = 3 to 4, 15 to 21 larvae). Embryos colonized for 1.5, 24 or 48 h were subjected to the indicated antibiotic challenge, or incubated in water for the control condition. Following this 30 min treatment, bacterial load per embryo was determined in both groups. Mann-Whitney test: ***P* < 0.01, ****P* < 0.001 and *****P* < 0.0001. Ratios were calculated regarding the median of the data set; thus there is no values for colistin at t1.5h as the median of the treated group is zero. (C) Efficacy of ofloxacin, an antibiotic known to enter eukaryotic cells with high efficiency, on strain B6513 (same analysis as in (B)). (D) Representative maximal projections of confocal images of infected Tg(*mfap4:mCherry-F*) larvae (all mCherry⁺), treated or not with ofloxacin at 24 hpi. For both conditions, the number of embryos with or without at least one event of intra-macrophage bacteria are indicated below the images. Among the ofloxacin-treated embryos, 2 were GFP-negative, indicative of bacterial elimination, whereas all non-treated embryos were GFP-positive. Drawings in panels A and D were created with BioRender.com.

<https://doi.org/10.1371/journal.ppat.1012922.g005>

µg/mL for tobramycin and 20 µg/mL for ciprofloxacin), except for colistin that was toxic for embryos at 40 x MIC, but 2.5 x MIC (10 µg/mL) was tolerated by the embryos. All drugs caused a sharp reduction in bacterial loads when applied soon after the initiation of infection (1.5 hpi), from approx. 20-fold (ciprofloxacin and tobramycin) to complete eradication (colistin) (Fig 5B). However, their efficacy was strongly reduced when used at 24 or 48 hpi, with colistin and ciprofloxacin decreasing CFU counts by less than 7-fold and tobramycin having no significant effect (Fig 5B). The ability of bacteria to withstand antibiotic challenges occurred at around the time of establishment of a persistent infection in the embryos, associated with intracellular and aggregated bacteria. This phenotype was not linked to the acquisition of mutations conferring resistance, since colonies isolated from embryos following ciprofloxacin or tobramycin challenge at 48 hpi remained as sensitive as the original B6513 to these antibiotics *in vitro* (see procedure in Methods section). Moreover, the adaptive resistance phenotype was not specific to isolate B6513 since a similar phenotype was found with RP73 strain upon treatment with colistin (S9 Fig).

During infection, *P. aeruginosa* may benefit from intracellular niches to escape antibiotics [8,11]. Our microscopy analysis revealed the intracellular localization of persistent *P. aeruginosa*, which could *de facto* be protected from antibiotics (Figs 2A–C, 3 and S7). Antipseudomonal antibiotics differ in their ability to penetrate into eukaryotic cells, and their activity vary against intracellular *P. aeruginosa* in cultured phagocytes [11]. To assess if the intracellular niche was responsible for the treatment failure in our model, we tested the *in vivo* activity of another fluoroquinolone, ofloxacin, that is known to be host cell permeable and to demonstrate better diffusion into human tissues than ciprofloxacin [38]. Persistent bacteria at 24 and 48 hpi exhibited some tolerance towards ofloxacin (used at 40 x MIC, 20 µg/mL), when compared to bacteria treated very early after the start of infection. However, among the four antibiotics tested, ofloxacin was the most efficient molecule at the persistent stages (24 and 48 hpi), thus reinforcing the notion that eradication of intracellular persistent bacterial reservoirs requires administration of antibiotics able to reach these niches (Fig 5C). To complete this finding, we imaged infected Tg(*mfap4::mCherry-F*) embryos at 24 hpi treated or not with ofloxacin (Fig 5D). The percentage of larvae with intra-macrophage bacteria dropped below 30% in ofloxacin-treated fishes, whereas it remained around 70% in non-treated controls (as seen in Fig 2G).

Taken together, our results showed that the persistence of *P. aeruginosa* in zebrafish embryos is associated with an adaptive phenotype of resistance to antibiotics. Importantly, the most cell-permeant antibiotic was also the most effective one, suggesting that intracellular bacteria are reservoirs resistant to antibiotics that do not enter host cells.

Anti-biofilm compounds potentiate antibiotic efficacy on persistent bacteria

In our zebrafish model, persistent *P. aeruginosa* formed aggregates, which may display a higher tolerance to antibiotics than free-living bacteria [7]. We hypothesized that anti-biofilm compounds would help to disassemble bacterial aggregates, thereby re-sensitizing persistent *P. aeruginosa* to antibiotics, potentially promoting their eradication with the assistance of the immune system. Among commercially available molecules with appealing activity against *P. aeruginosa* biofilm, we first used the human Atrial Natriuretic Peptide (hANP), an efficient biofilm-disperser *in vitro* that potentiates different antibiotics including tobramycin [39]. Though devoid of antibacterial activity by itself, peptide hANP was able to reduce the formation of biofilms by strain B6513 *in vitro* (S10 Fig). We then assessed its capacity to potentiate tobramycin and colistin treatments in infected embryos at 48 hpi, a time point at which

bacteria were partly tolerant to antibiotics (Fig 6A). When applied alone, hANP modestly reduced bacterial loads by 2.5-fold, suggesting that it somehow assisted the innate immune system to eliminate bacteria. Strikingly, when used in combination with antibiotics, a more significant reduction of the pathogen burden was recorded, i.e., 7-fold for tobramycin and 16-fold for colistin, when compared with the controls (Fig 6B). We performed similar experiments with a structurally different anti-biofilm compound, the fatty acid *cis*-2-Decenoic acid (CDA). CDA, a molecule produced by *P. aeruginosa*, promotes biofilm dispersal and potentiates clearance of pre-established biofilms in combination with antibiotics [40,41]. Moreover, CDA was proposed as a suitable molecule to target intra-macrophagic biofilms of pathogenic *Escherichia coli* [42]. When used alone at 48 hpi, CDA had no detectable effects on persistent *P. aeruginosa* in zebrafish embryos, but when added in combination with colistin, bacterial loads per embryo decreased by 5-fold, thus increasing the antibiotic efficacy by > 3-fold (Fig 6C).

We also tested the anti-biofilm compounds (hANP or CDA) in combination with the most potent antibiotic, ofloxacin. However, the anti-biofilm compounds did not improve the ofloxacin efficacy, which may be due to the fact that dispersed bacteria may be poorly susceptible to ofloxacin due to metabolic issues. Alternatively, it may be due to the fact that most bacterial aggregates are intracellular, possibly inside vacuoles, and may reflect an insufficient penetration of anti-biofilm molecules.

We next took advantage of the optical transparency of embryos to visualize *in vivo* the effect of these anti-biofilm molecules on persistent bacteria. After a 5 h exposure to hANP or CDA, a reduction of the size of some bacterial clusters and concomitant increased number of isolated bacteria were observed, which was not the case in the H₂O control conditions (Figs 6D and S11). In the few treated embryos that were imaged, we did not observe the dispersion of intra-macrophage bacterial clusters. The ability of hANP and CDA to enter cells and cross membrane vacuole in our working conditions remains unknown. Currently, we cannot determine if anti-biofilm molecules act on intracellular and/or extracellular bacteria because Tg(*mfap4::mCherry-F*) labeling do not allow to distinguish extracellular bacteria from intracellular bacteria residing in non-macrophage cells. One can also hypothesize that bacterial clusters from damaged cells would be more accessible to these molecules.

Cumulatively, these results are consistent with the notion that persistent *P. aeruginosa* bacteria present in aggregated structures, which are dispersible upon addition of anti-biofilm molecules, contribute to the adaptive antibiotic-resistant phenotype. Moreover, these findings validate the pertinence of our *in vivo* model to identify compounds that could potentiate the effects of conventional antibiotics.

Discussion

Modeling bacterial chronic infection *in vivo* is essential to understand pathogenesis and evaluate treatment efficacy in a context that includes responsive host innate immunity and tissues. Here, we propose an *in vivo* model, complementary to mouse models, based on the infection of wounded zebrafish embryos with *P. aeruginosa* clinical strains. This model showed the utility of CF isolates in establishing a persistent wound infection suitable for drug testing and provided novel information on *P. aeruginosa* persistence in an intracellular niche, evading antibiotic treatment. Indeed, the zebrafish embryo model provides unique opportunities for intravital imaging and highlights the importance of an intracellular phase for establishing bacterial persistence in a vertebrate host. Moreover, this model recapitulates a major feature of chronicity, i.e., adaptive antibiotic resistance, and allows a simple screen for compounds that re-sensitize bacteria to antibiotics.

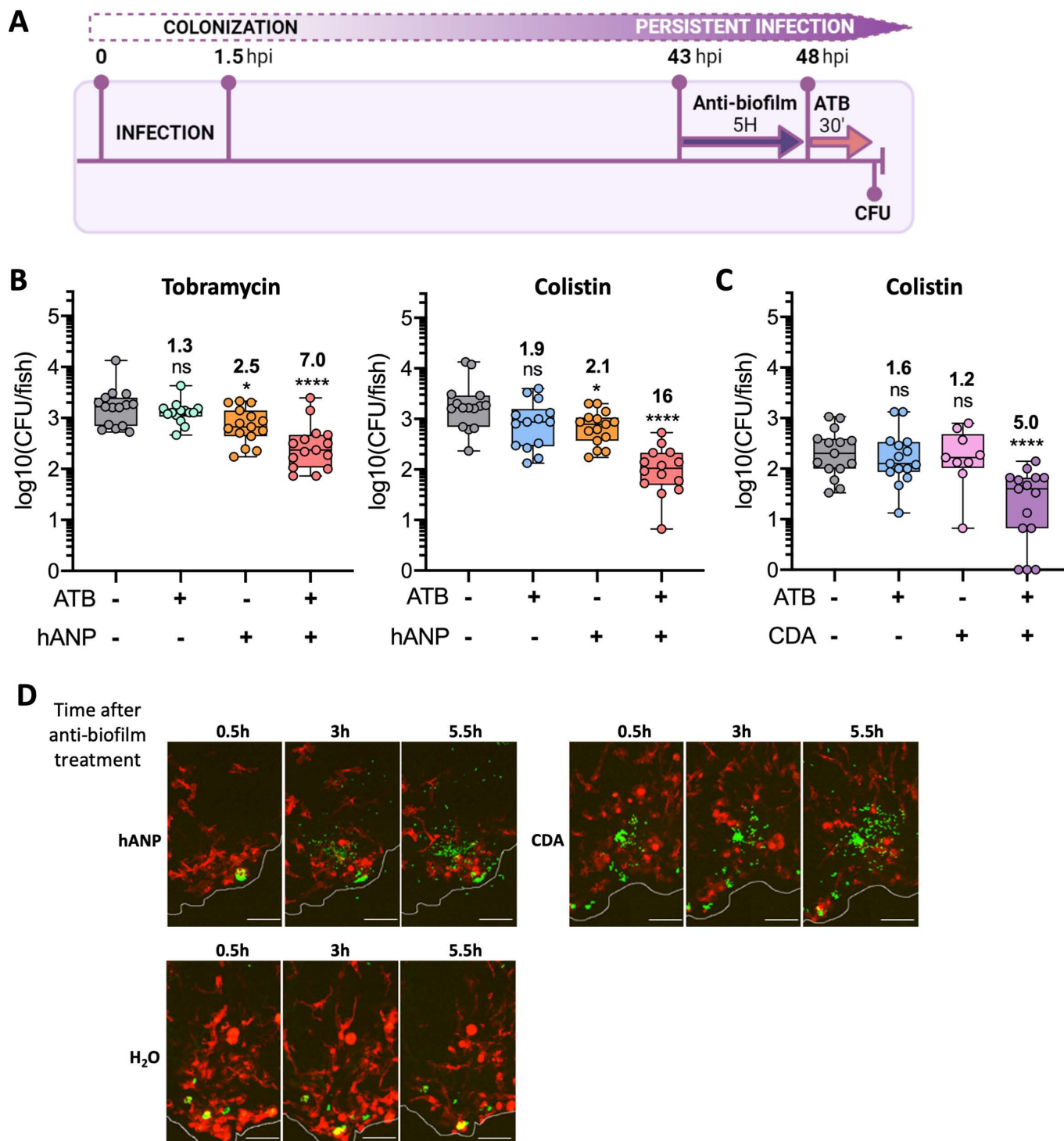


Fig 6. Treatment with anti-biofilm compounds can re-sensitize persistent *P. aeruginosa* bacteria to antibiotics in infected zebrafish. (A) Experimental procedure to assess the combine effect of anti-biofilm molecules and antibiotics. ATB 30': antibiotic treatment for 30 min. Drawing was created with BioRender.com. (B) and (C) Antibiotic potentiation by 10 μ M hANP (B) and 20 μ M CDA (C) at 48 hpi ($n = 2$ or 3, 9 to 15 larvae). Anti-biofilm compounds were added for 5 h to embryos infected by B6513-gfp strain, followed by the indicated antibiotic treatment, before CFU counting per embryo. One-way ANOVA: **** $p < 0.0001$; Dunnett post-hoc test (comparison with the control condition): * $P < 0.05$, ** $P < 0.01$ and **** $P < 0.0001$. Ratios were calculated regarding the median of the data set. (D) Maximal projections of confocal images, showing the effect of hANP or CDA following the treatment used in (B) and (C), without antibiotic treatment. Pictures of Tg(*mfp4:mCherry-F*) larvae infected by strain B6513-gfp were taken, from the beginning of the treatment, every 30 min for 5.5 h. A selection of images at 3 time points is shown. Scale bar: 40 μ m.

<https://doi.org/10.1371/journal.ppat.1012922.g006>

To establish this first model of persistent *P. aeruginosa* infection in zebrafish, we combined different parameters that have not been tested with clinical isolates to date: (i) parallel analysis of several *P. aeruginosa* isolates from CF patients, including a reference isolate known to establish a long-term pulmonary infection in a murine model [25], (ii) experiments over a period of up to 3 days after infection, and (iii) wound infection. The bacterial isolates could not be differentiated in this model based on the mortality rate of embryos since, in contrast to PAO1 strain, the mortality was very low or absent with the four isolates tested. However, the analysis over a 3 day period allowed us to clearly distinguish two classes of strains, those being persistent (B6513 and RP73) and those that were eliminated. Notably, the virulence and bacterial load profiles of clinical isolates in zebrafish matched well the profiles observed in a mouse model of chronic wound infection, further validating the physiological relevance of our non-mammalian model. This is in line with recent studies that developed persistent *Shigella* or *Salmonella* infections in the zebrafish embryo [43,44]. In our work, B6513 strain was used in microscopy analysis and treatment assessment, but key findings (persistence, intra-macrophage location and antibiotic tolerance) were also validated with the RP73 strain, a CF isolate known to persist in mice model. Further studies will be required to investigate intracellular *P. aeruginosa* in mice and human wounds.

The zebrafish embryo offers unique advantages to track bacterial infections in real time, and to study the interaction between bacteria and host cells. In keeping with previous studies using other infection routes, intravital microscopy revealed that infecting *P. aeruginosa* introduced at the tail injury were phagocytosed by both neutrophils and macrophages shortly after infection [20,45]. While neutrophils were still present at the injury site at later time points, they rarely interacted with persistent *P. aeruginosa*, as opposed to macrophages. Unexpectedly, persistent bacteria were often visualized inside macrophages, which are long-living cells, indicating that *P. aeruginosa* displays strategies to resist macrophage killing and can use macrophages as a persistence niche. Such strategies are hallmarks of diverse intracellular pathogens, and were not expected for *P. aeruginosa*, which is considered an extracellular bacterium. This is however consistent with our findings highlighting an intra-macrophage stage in cellular models and during *P. aeruginosa* acute infection [20,34,35]. In addition, we recently reported that strain PAO1 can persist at low levels in microinjected larvae that overcome or do not develop an acute infection, with some persistent bacteria also visualized inside macrophages [24], and similar findings were observed in the present study upon infection of wounded embryos with PAO1. Here high-resolution imaging of infected zebrafish using EM confirmed that persistent B6513 bacteria often reside inside host cells. Intracellular persistent bacteria were also visualized in non-phagocytic cells, supporting the importance of invasion of non-phagocytic cells during infection [46,47]. Whereas the intracellular location of *P. aeruginosa* during infection was first reported three decades ago [33] and despite numerous studies on *P. aeruginosa* life inside cultured epithelial cells [9], its relevance *in vivo* has been a matter of debate and its role in persistence *in vivo* has not been addressed to date. Importantly, recent studies using intravital confocal imaging of infected mouse corneas and confocal imaging of human lung explants from CF patients support the intracellular location of *P. aeruginosa* during infection, as individual bacteria or small bacterial clusters [10,46]. The nature of cells harboring *P. aeruginosa* was however not ascertained in these studies and, in this regard, the zebrafish model is a unique model, complementary to mice and human studies, that enables monitoring the dynamics of intracellular *P. aeruginosa* *in vivo*. Intra-animal high resolution correlative microscopy (CLEM) in zebrafish allowed us to image for the first time an intra-macrophage *P. aeruginosa* cluster. Moreover, real time imaging demonstrated that such clusters can last for more than 10 hours inside macrophages. The finding of an intracellular

bacterial reservoir is consistent with the persistence pattern of some clinical *P. aeruginosa* CF isolates upon long-term infections of airway epithelial cells [48,49].

Our previous studies with PAO1 derived strains infecting cultured macrophages showed diverse outcomes, including intracellular bacteria that reside in vacuoles or in the cytoplasm [24,34]. We observed here a vacuolar location for isolate B6513 upon infection of a macrophage cell line, and high-resolution EM imaging from infected zebrafish confirmed that individual or clustered persistent bacteria can reside inside host cell vacuoles *in vivo*. This is in line with the recent finding of a vacuolar persistent subpopulation of intracellular *P. aeruginosa* in cultured epithelial cells and the intravital imaging of colored puncta considered as vacuolar bacterial clusters during corneal infection [46]. A vacuolar location should contribute to clustering of bacteria, which may retain a clustered structure in case of vacuolar rupture. Some clusters of persistent *P. aeruginosa* visualized in zebrafish had sizes above 10 μm , which is in line with aggregates found in CF lungs and chronic wounds [50,51] that are considered to represent non-attached biofilm-like structures [52]. Of note, the bacterial aggregates observed in zebrafish could be dispersed, with a concomitant increase in isolated bacteria, upon addition of two different anti-biofilm molecules, hANP or CDA. Real time imaging of the dispersion of bacterial aggregates in a living animal demonstrates the unprecedented benefits of zebrafish embryo to follow the dynamics of bacterial clusters *in vivo*.

Persistent bacteria in the zebrafish model were refractory to antibiotic challenge, which mimics bacterial behavior during chronic infection in mammals and humans [53]. Such adaptive antibiotic resistance of bacteria has been attributed to several features, including biofilm structures, which are well documented *in vitro* for *P. aeruginosa* [7]. Here, the aggregated bacteria visualized *in vivo* appeared to contribute to adaptive resistance since anti-biofilm compounds could significantly re-sensitize persistent bacteria to antibiotic treatment. The bacterial intracellular stage is another feature allowing evasion of antibiotic challenge that recently attracted interest in the case of extracellular pathogens as *P. aeruginosa* [8,54]. For example, the residence inside cultured lung epithelial cells reduced antibiotic efficiency [12,55] and intracellular *P. aeruginosa* in bladder epithelial cells promoted bacterial persistence and antibiotic tolerance in a mouse model of urinary tract infection [13]. In our zebrafish model, the observation that the most efficient cell-permeant antibiotic, ofloxacin, demonstrated the highest efficacy supports the idea that the intracellular location provides a niche where persisting bacteria are less accessible to antibiotics. Ofloxacin, remains however only partially efficient against persistent bacteria, which may correlate with a poor efficacy against bacteria with a vacuolar location, which would further protect bacteria from antibiotics [46].

Finding new therapeutics to tackle chronic infections is critical and we provide a new platform to screen and evaluate *in vivo* the efficacy of treatments against persistent *P. aeruginosa*. Our model underscores the importance of strategies efficiently targeting the protective intracellular niche, which plays a crucial role in sustaining persistence within the host animal. This was not obvious for a pathogen such as *P. aeruginosa* which has been considered to be largely extracellular, but was consistent with the importance of an intra-macrophage stage during infection for other major pathogens considered as extracellular pathogens, including *Acinetobacter baumannii* and *Streptococcus pneumoniae* [56,57]. Other extracellular pathogens responsible for respiratory diseases, as *Staphylococcus aureus*, *Bordetella pertussis* and *Haemophilus influenzae* also experience intracellular phases [54]. Additionally our *in vivo* model reinforces the relevance of anti-biofilm strategies that disperse bacterial aggregates to re-sensitize *P. aeruginosa* to antibiotic treatments. This zebrafish model offers the possibility of insightful therapies, especially combination of treatments, that could be transposed and refined in mammalian models, including man. Integrating studies in zebrafish and mouse models should greatly accelerate the identification of efficient treatments against *Pseudomonas*. It will also

allow better understanding of the contribution of intracellular stages prior to the formation of biofilm-like structures in models of *P. aeruginosa* chronic infection.

Materials and methods

Ethics statement for zebrafish

All zebrafish experiments described in the present study were conducted at the University of Montpellier by following the 3Rs -Replacement, Reduction and Refinement- principles according to the European Union guidelines for handling of laboratory animals (https://environment.ec.europa.eu/topics/chemicals/animals-science_en) and were approved by the “Direction Sanitaire et Vétérinaire de l’Hérault” and the “Comité d’Ethique pour l’utilisation d’animaux à des fins scientifiques” under reference CEEA-LR-B4-172-37. Breeding of adult fish adhered to the international guidelines specified by the EU Animal Protection Directive 2010/63/EU. All experiments were performed before the embryos free feeding stage (5 dpf) and did not fall under animal experimentation law according to the EU Animal Protection Directive 2010/63/EU. Embryos were euthanized using the anesthetic tricaine up to a lethal dose before bleach treatment. Embryo manipulation, handling, and euthanasia were performed by well-trained and authorized staff. Embryos were euthanized using an anesthetic overdose of buffered tricaine before bleach treatment.

Clinical strains used in the study and growth conditions

P. aeruginosa clinical strains were routinely grown at 37 °C in lysogeny broth (LB) with shaking at 180 rpm. Clinical strains A6520, B6513 and C6490 were isolated at the teaching hospital of Besançon (France) from three individual cystic fibrosis patients aged 4, 1 and 17 years, respectively showing a transient (A6520, B6513) or chronic (C6490) lung colonization with *P. aeruginosa*. As recommended by international guidelines, all these cystic fibrosis patients were repeatedly treated with combinations of antibiotics to control or attempt to eradicate their pulmonary infection (individual treatment regimens were not available). Genome sequencing was carried out to classify the strains. Sequence Types (STs) were determined according to the MLST scheme available at PubMLST (<https://pubmlst.org>). Strains A6520, B6513 and C6490 were found to belong to the same phylum as reference strain PAO1 [58], to harbor the exotoxin-encoding gene *exoS*, and to be genotypically distinct (ST274, ST27 and ST633, respectively). This Whole Genome Shotgun project (whole genomes sequences of the clinical isolates) has been deposited at DDBJ/ENA/GenBank under the accession JAWDIG000000000 (A6520), JAWDIH000000000 (B6513) and JAWDII000000000 (C6490). RP73 is a well described CF *P. aeruginosa* [26].

Chemicals

All antibiotics were purchased from Sigma-Aldrich. Ciprofloxacin was dissolved at 25 mg/mL in 0.1 M hydrochloric acid. Ofloxacin was dissolved at 20 mg/mL in 1 M NaOH. Colistin sulfate salt and Tobramycin were dissolved at 8 mg/mL in ultrapure water. The human Atrial Natriuretic Peptide (hANP) was purchased from Tocris Bioscience (Bio-Techne) and was dissolved at 1 mg/mL in ultrapure water and stored at −20 °C. The *cis*-2-Decenoic acid (CDA) was purchased from Sigma-Aldrich and was dissolved at 5.8 mM in 100% DMSO and stored at −20 °C.

Minimum inhibitory concentration (MIC) assays

Susceptibility levels of strain B6513 to the fluoroquinolones ciprofloxacin (0.5 µg/mL) and ofloxacin (0.5 µg/mL), the polymyxin colistin (4 µg/mL), and the aminoglycoside tobramycin

(1 µg/mL) were determined by the standard microdilution method in 96-well plates. Overnight cultures in LB broth were diluted in the same medium to an initial inoculum of $OD_{600nm} = 0.1$. MIC was defined as the lowest concentration that inhibited bacterial growth.

Construction of stable fluorescent *P. aeruginosa* strains

Strains with chromosomally encoded GFP were obtained by triparental mating by using a recombinant integrative plasmid miniCTX carrying the PX2-GFP fusion [59] (from Ina Attree, Université Grenoble Alpes, France). Following overnight growth in LB broth with appropriate antibiotics, *E. coli* TOP10 carrying either helper plasmid pRK2013 [35] or miniCTX-PX2-GFP were mixed (20 µL of each culture) and deposited as drops onto the surface of LB plates for 2 h at 37 °C. In parallel, the overnight cultures of *P. aeruginosa* strains were incubated at 42 °C. 20 µL fractions of these stationary phase cultures were then individually added to the *E. coli* dry drops and left at 37 °C for 5 h. The bacterial spots were then scrapped off and directly plated on LB plates containing Irgasan (25 µg/mL) and tetracycline (from 50 to 200 µg/mL) to select *P. aeruginosa* transconjugants. After 18 h at 37 °C, several colonies were streaked out on LB medium to verify the stable GFP expression, and an individual GFP⁺ colony was cultured in liquid LB to obtain a glycerol stock.

Zebrafish lines

Wild-type AB and Golden lines or AB/Golden mixed genetic background zebrafish were used for survival and CFU experiments. For live imaging, lines carrying fluorescent macrophages Tg(*mfap4:mCherry-F*)ump6TG [60], neutrophils Tg(*LysC:dsRed*)nz50 [61] or mesenchymal cells Tg(*rcn3:Gal4/UAS:mCherry*) [62,63] were used. Fish maintenance, staging and husbandry were performed as described [64]. Eggs were obtained by natural spawning, collected in petri dishes and incubated at 28°C in fish water composed of 60 µg/mL sea salts (Instant Ocean) in distilled water supplemented with 0.4 mM NaOH and 0.1% methylene blue. Embryos and larvae were staged according to [65]. For experiments, larvae were used at 2-day post-fertilization (dpf) until 5 dpf.

Infection by immersion of injured zebrafish embryos

The protocol was essentially as described earlier [23], with few modifications. Overnight bacterial cultures were diluted at 1:20 in fresh LB broth and incubated until the OD_{600nm} reached approx. 0.8–1. Cultures were centrifuged at 4000 rpm for 10 min and re-suspended in fish water at approx. 10^7 bacterial/mL. The bacterial load was determined by subsequent plating onto LB agar after dilution into phosphate-buffered saline (PBS). 2 dpf embryos, previously dechorionated, were anesthetized with tricaine (300 µg/mL, Sigma-Aldrich) and injured at the tail fin using 25-gauge needles under a stereomicroscope (Motic). Embryos were distributed into a 6-well plate containing 4 mL of bacterial suspension (or fish water as a control) immediately after the injury, and incubated at 28 °C for 1.5 h. Two washes in fish water were subsequently performed (30 min in 10 mL and a few minutes in 4 mL, respectively) to eliminate bacteria in the bath. Finally, larvae were transferred individually into a 96-well plate (survival experiment) or a 24-well plate (CFU measurement and microscopy) containing fish water, and incubated using a light/dark cycle at 28 °C. For survival curves, death was determined based on the absence of heart beat after visual inspection.

Bacterial load measurement in infected embryos

Before CFU quantification, infected embryos were washed for a few minutes in 4 mL of fish water and subsequently crushed individually using a pestle in 100 µL of PBS. Then 100 µL of

Triton X-100 (1% final concentration) were added for 10 min to liberate bacteria from residual cells/tissues. Following lysis, several dilutions in PBS were spotted on LB agar plates and incubated approx. 18 h at 37 °C. Only GFP⁺ colonies were considered for counting. For CFU measurement following treatment, embryos were washed before the treatment and not prior the crushing (see below). The number (n) indicated in figure legends reflects the number of independent experiments.

Embryo imaging

After reaching the 50% epiboly stage, embryos were maintained in fish water supplemented with the melanization inhibitor Phenylthiourea (PTU) to prevent pigmentation. Before imaging, larvae were anesthetized with 300 µg/mL tricaine and placed in 35 mm glass-bottom dishes (FluoroDish, World Precision Instruments) and immobilized with 1% low-melting-point agarose (Sigma-Aldrich), covered with fish water after solidification. Zebrafish larvae were imaged at indicated hpi using the ANDOR CSU-W1 confocal spinning disk on an inverted NIKON microscope (Ti Eclipse) with ANDOR Zyla 4.2 sCMOS camera (40x water/NA 1.15 objective). Optimal laser power and exposure times were determined for each strains (GFP) and cell types (mCherry), and were identical between independent experiments. Settings of brightness and contrast used for a better visualization were the same between all independent experiments. The 3D files generated by multi-scan acquisitions were processed using Image J and compressed into maximum intensity projections. Brightness and contrast were adjusted for better visualization. Deconvolution of images was done to improve resolution with Huygens (SVI).

Quantification of macrophage recruitment, bacterial volumes and percentage of intra-macrophage GFP⁺ foci

As a proxy to quantify macrophage recruitment at the injury site following spinning disk confocal imaging, the area formed by positive pixels (mCherry⁺) was measured at the median plan of each stack. To that aim, using Fiji, a threshold of positivity was applied using the "Iso-Data" method. 3D reconstructions and volume quantification of GFP⁺ events were performed using the Imaris "surface" tool. Following the generation of GFP⁺ 3D objects, very small events (volume <0.5 µm³) with non-rod shapes were considered as autofluorescence and eliminated. In addition, rare GFP⁺ objects localized outside the tissues (e.g., at the surface of the fish) were manually removed from the analysis.

Quantification of the percentage of GFP⁺ foci located inside macrophages over time was performed on embryos with at least one event of intra-macrophage foci (7 to 11 embryos at each time point). Confocal Z-stacks were converted into maximal intensity projections (MIP) in the GFP channel and a threshold was applied on the 2D images at a pixel value two times higher than the background value. Using a composite GFP/mCherry Z-stack in parallel, GFP⁺ foci identified on the MIP were localized outside or inside macrophages and grouped in the ROI manager to measure their surface. A global "GFP area" was calculated before deducing the percentage of intra-macrophage surface.

Treatment of infected embryos with antibiotics and anti-biofilm molecules, and assessment of antibiotic resistance of bacteria recovered from antibiotic treated animal

Prior any treatment, embryos were systematically washed for a few minutes in 4 ml of zebrafish water. Infected larvae were incubated with 40 x MIC of antibiotics, except for colistin (2.5 x MIC). Depending of the antibiotic, controls were done with fish water alone or

supplemented with NaOH or HCl at the proper concentration. At least 5 embryos of the same condition were treated together for 30 min in 1 mL at room temperature. For CDA (20 μ M) and hANP (10 μ M), treatments were applied individually for 5 h at 43 hpi in 200 μ L at 28 °C. Control conditions were fish water alone (hANP) or supplemented with 0.34% DMSO (CDA). Independent experiments were systemically performed 3 times, with at least 5 larvae per condition (i.e., minimum 15 embryos in total).

Bacteria recovered from antibiotic treated animals at 48 or 72 hpi were challenged against antibiotics *in vitro* to assess if bacteria acquired antibiotic resistance. Bacteria recovered from CFU plating were grown O/N in LB medium in parallel with an *in vitro* colony (not obtained from zebrafish infection). Bacterial cultures were treated with ciprofloxacin (20 μ g/ml) or tobramycin (20 μ g/ml) for 30 min and the susceptibility to antibiotics was determined by surviving CFU. Bacteria issued from embryos (3 independent colonies tested) were as sensitive as the original B6513.

Cutaneous infection in mice

Animal experiments were performed in accordance with the Canadian Council on Animal Care (CCAC) guidelines and were approved by the University of British Columbia Animal Care Committee protocol (A23-0030). Mice used in this study were outbred CD-1 mice (female). All animals were purchased from Charles River Laboratories, Inc. (Wilmington, MA, United States) and were 7–8 weeks of age at the time of experiments. Mice weighed 25 ± 2 g at the experimental start point and standard animal husbandry protocols were employed.

We tested the virulence of *P. aeruginosa* clinical isolates (A6520, B6513, and C6490) and the Liverpool Epidemic Strain LESB58 in a nuanced model of cutaneous high-density infection as previously described [16] with minor modifications. All strains were sub-cultured at 37°C with shaking (250 rpm) to an $OD_{600nm} = 1.0$ in LB. Cells were washed twice with sterile phosphate buffered saline (PBS) and resuspended to a final $OD_{600nm} = 0.5$ or 1.0 for clinical isolates or LESB58 strains, respectively. Strains were used to form high-density abscess infections to model invasive or chronic infections. Abscesses were formed by injection of 50 μ L of bacteria on the left dorsum of mice for 3 or 7 days. Disease progression and overall welfare of animals was monitored daily up to day three, and weekly thereafter. At experimental endpoint, animals were euthanized using carbon dioxide followed by cervical dislocation, and abscess lesion size was measured using a caliper. Abscesses were harvested in PBS and homogenized using a Mini-Beadbeater (BioSpec Products, Bartlesville, OK, United States) for bacterial enumeration on LB. Two independent experiments containing 2–4 biological replicates each were performed.

Electron microscopy

Samples were chemically fixed using 2.5% glutaraldehyde (Electron Microscopy Sciences # 16216) in fish water. After fixation, embryos were stored at 4 °C in the fixation solution until subsequent processing. The procedure for embedding in resin was adapted from a previous method [66]. All the procedure, except the overnight incubation in uranyl acetate, was performed using a Pelco Biowave PRO+ Microwave processing systems (TED Pella) following the program indicated in Table S1. Samples were post-fixed with 2% osmium tetroxide (O_8O_4) in 0.1M cacodylate buffer pH 7.4 containing 5 mM $CaCl_2$, immediately followed by 1.5% K-ferrocyanide in the same buffer. After washing, samples were treated with 1% thio-carbohydrazide at 60 °C, washed with distilled water before a second incubation in 2% OsO_4 . After washing, samples were then incubated overnight in 1% uranyl acetate at 4 °C. Samples were next heated at 40°C and further processed in the microwave (Table S1), washed and incubated in lead aspartate pre-heated at 50°C. Dehydration was performed with growing

concentrations of acetonitrile. Samples were then impregnated in Epon Hard+(TM) resin, and polymerized 48 h at 60 °C. All chemicals were from EMS.

Thin serial sections were made using an UCT ultramicrotome (Leica) equipped with a Jumbo ultra 35° diamond knife (Diatome). Section ribbons were collected on silicon wafers (Ted Pella) with the help of an ASH2 manipulator (RMC Boeckler). Sections were imaged with a Zeiss Gemini 360 scanning electron microscope on the MRI EM4B platform under high vacuum at 1.5kV. Final images were acquired using the Sense BSD detector (Zeiss) at a working distance between 3.5 and 4mm. Mosaics were acquired with a pixel size of 5 nm and a dwell time of 3.2 μs.

Macrophage infection and quantification of intracellular bacteria

J774 cells (murine macrophage cell line) were maintained at 37 °C in 5% CO₂ in Dulbecco's modified Eagle medium (DMEM, Gibco) supplemented with 10% heat-inactivated fetal bovine serum (FBS, Gibco). The infection of J774 macrophages by *P. aeruginosa* was carried out essentially as described previously [35]. J774 macrophages (5 x 10⁵ cells/well) were infected by mid-log phase bacteria in PBS, at a MOI of approx. 10. Infection synchronization was done by a 5 min centrifugation at 1000 rpm of the 24-well plate, and bacterial phagocytosis was allowed to proceed for 25 min. Cells were then washed three times with sterile PBS and fresh DMEM medium supplemented with 400 μg/mL gentamicin was added, which was retained throughout the infection to kill non-phagocytosed bacteria. Macrophages were lysed after 20 min (T0) or 2 h (T1) of gentamicin treatment, by using 0.1% Triton X-100 and the number of viable bacteria was determined by subsequent plating onto LB agar plates. Survival rate at T1 was compared to the number of internalized bacteria at T0. The cytotoxicity driven by internalized bacteria was assessed using Trypan blue as described [34].

Live microscopy on cultured macrophages

J774 macrophages were seeded in glass bottom 8 wells μ-slide (Ibidi #80827) in DMEM medium supplemented with 10% FBS and infected with *P. aeruginosa* strains expressing GFP as described above. Imaging started after 30 min of phagocytosis, when the media was changed to DMEM supplemented with 400 μg/ml gentamicin until 3 h post phagocytosis. Cells were imaged using an inverted epifluorescence microscope (AxioObserver, Zeiss), equipped with an incubation chamber set-up at 37 °C and 5% CO₂ and a AxioCam 503 Mono camera (Photometrics). Time-lapse experiments were performed, by automatic acquisition of random fields using a 63X Apochromat objective (NA 1.4). The frequency of acquisition is indicated in figure legends. Image treatment and analysis were performed using Image J.

Biofilm formation

Biofilm formation was assessed in low magnesium medium in glass tubes 24 h at 30 °C under static condition as described previously [67]. After 24h, bacterial growth was measured by OD_{600nm} and tubes were carefully washed with water. The biofilm at the air-liquid interphase was stained using crystal violet (CV) 0.1% during 15 min at room temperature. After staining, tubes were washed with water and CV was extracted using acetic acid (30%) and quantified by measuring the OD_{570nm}.

Swarming motility

A modified form of basal medium (BM2) consisting of 62 mM potassium phosphate buffer (pH = 7.0), 2 mM MgSO₄, 10 μM FeSO₄, 20 mM glucose and 0.1% casamino acids (CAA) was used for swarming assays. Subcultures were adjusted to a starting OD₆₀₀ = 0.1 in BM2 and grown to an OD_{600nm} = 0.4–0.6 for spot inoculation on solidified medium (0.4% agar). Plates were incubated

for 18–24 h at 37 °C, were imaged with a BioRad ChemiDoc and surface area coverage of the plate was measured in ImageJ2 software (v2.14.0). Three biological replicates were examined.

Pyocyanin production

The concentration of pyocyanin in bacterial supernatants was determined spectrophotometrically after extraction with chloroform and 0.2 M HCl, as described elsewhere [68]. Absorbance at 520 nm was read using a Biotek Synergy H1 Microplate Reader. Three biological replicates were examined.

In vitro efficiency of hANP

The flow cell system, which allows for continuous bacterial biofilm formation, is assembled, prepared and sterilized as described earlier [69]. For studying the impact of hANP peptide on established strain B6513 biofilm, we used an established protocol [39]. Briefly, bacterial cells from an over-night culture, were recovered by centrifugation (10 min, 7,500 rpm) and washed with sterile physiological water (0.9% NaCl). Each channel of the flow cell (1 mm x 4 mm x 40 mm, Bio centrum, DTU) was inoculated with 300 μ L of bacterial suspension prepared at an optical density of $OD_{580nm} = 0.1$. Bacterial adhesion was allowed without any flow for 2 h at 37 °C. After 2 h of adhesion, the LB medium was pumped with a flow rate of 2.5 mL/h at 37 °C for 24 h. Next, the 24 h-old biofilm was exposed for 2 h to 300 μ L of hANP (0.1 μ M) or 300 μ L of ultra-pure distilled water (control condition), added to each channel of the flow cell and without flow. Prior to image acquisition, biofilm cultures were then rinsed with LB medium using a 2.5 mL/h flow rate for 15 min. Finally, bacterial cells were marked with 5 μ M of SYTO9 green-fluorescent dye (Invitrogen) and observed using confocal laser scanning microscopy (CLSM). CLSM observations of biofilms were performed using a Zeiss LSM710 microscope (Carl Zeiss Microscopy) using a x40 oil immersion objective. In order to capture the entire biofilm depth, images were taken every millimeter. For visualization and processing of three-dimensional (3D) images, the Zen 2.1 SP1 software (Carl Zeiss Microscopy) was used. Using the COMSTAT software (<http://www.imageanalysis.dk/>), quantitative analyses of image stacks were carried out [70].

Statistical analysis

GraphPad Prism 8.3.0 was used to perform all statistical tests and create graphs. The box plots represent the median, as well as min and max values with the interquartile range. The indicated test used to analyze each dataset was chosen depending on the normality of the data. Multiple comparisons were done by one-way ANOVA or Kruskal-Wallis test, followed by Tukey's or Dunn's pairwise comparison, respectively. The Dunnett's many-to-one comparison was used following a one-way ANOVA. Mann-Whitney U test was used to compare two groups.

Supporting information

S1 Fig. Persistent isolates colonize the wound but not the skin of the embryos. Uninjured larvae were immersed with GFP⁺ persistent isolates B6513 and RP73, and were subsequently crushed and plated for CFU counting over approx. 72 hpi (n = 3, 15 larvae). The difference between B6513 and RP73 at time 1.5 h in uninjured embryos may reflect different ability of the strains to adhere to embryos (of note, the number of CFUs of RP73 at time 1.5 h in uninjured embryos is much lower compared to injured embryos in [Fig 1C](#)). (PPTX)

S2 Fig. Clinical scores of mice infected with the different *P. aeruginosa* clinical strains.

Clinical welfare of animals used in the murine model of high-density cutaneous infection was monitored using a standardized scoring system for assessing disease severity. Mice were monitored daily for the first three days post-infection (dpi), then weekly thereafter. Scores were assigned for a pre-determined battery of traits, including activity, hydration, pain, injection site, etc. and then summated for each animal. Strain B6513 did cause mortality of one animal at two dpi (out of 14 infected mice), though the cause of death was not determined as total necropsy could not be performed prior to rigor mortis. Data are expressed as the mean clinical score for all animals in each treatment group +/- the standard error of the mean (SEM) ($n = 5-7$).

(PPTX)

S3 Fig. Sequential Z stack slices of a 3D reconstitution to confirm the intramacrophage location of a bacterial foci. The images were used for the 3D reconstitution shown in Fig 2B, representing a bacterial foci observed at t23h. The step between each optical section is 1 μm . (TIFF)

S4 Fig. Interaction of persistent RP73 and PAO1 strains with macrophages. Maximal projections of confocal images, showing interactions between bacteria (green) and recruited macrophages (red) in Tg(*mfap4:mCherry-F*) larvae. Boxed macrophages with intracellular *P. aeruginosa* were extracted from a single optical sections. Below the image (infected embryos), orthogonal representation of the (*) event is shown, confirming that bacteria are inside the macrophage. (A) Left panel: embryo infected with strain RP73 at 48 hpi. Right panel: non-infected embryo. Due to a low GFP expression by strain RP73, the exposure time was increased for imaging, generating higher autofluorescence signal (mainly around the notochord). The green signal specific to bacteria was however clearly discriminated from autofluorescence based on shape, intensity, localization at the injury site and comparison with uninfected control. (B) Two larvae infected with PAO1 were imaged at 24 hpi. Events with intramacrophage bacteria are quite rare, possibly due to the lower number of persisting bacteria and/or the higher cytotoxicity of intracellular PAO1 bacteria. Scale bar: 40 μm .

(PPTX)

S5 Fig. Visualization of macrophages at the site of injury. Maximal projections of confocal images, showing macrophages (red) in Tg(*mfap4:mCherry-F*) larvae which were injured but not infected (top) or infected but without intramacrophage bacteria detected at the time of imaging (bottom). Below the images, orthogonal representations of two events (indicated by white arrows) showing that the apparent yellow color of bacterial clusters in the maximal projection does not reflect an intramacrophage localization. Scale bar: 40 μm .

(PPTX)

S6 Fig. Visualization of neutrophils at the site of injury. Maximal projections of confocal images, showing neutrophils (red) in Tg(*LysC:dsRed*) larvae which were injured but not infected (top) or infected with intraneutrophilic bacteria detected at the time of imaging (bottom). Below the images, orthogonal representations of the (*) boxed events, confirming that bacteria were intracellular. Scale bar: 40 μm .

(PPTX)

S7 Fig. Interaction of persistent *P. aeruginosa* B6513 with non-phagocytic cells. Representative maximal projections of confocal images, showing interactions between bacteria (green) and mesenchymal cells (red) in Tg(*rcn3:Gal4/UAS:mCherry*) larvae at different time points. Boxed cells with intracellular *P. aeruginosa* were extracted from a single optical section. Below

the images, orthogonal representations of the (*) boxed events, confirming that bacteria were intracellular. Scale bar: 40 μm . Note that pictures come from different embryos imaged for each indicated times.

(PPTX)

S8 Fig. Swarming motility and pyocyanin production of *P. aeruginosa* strains. (A) Representative images of swarming motility on basal medium (BM2) supplemented with 0.1% casamino acids and 0.4% agar for *P. aeruginosa* clinical isolates and reference strain PAO1. Images were captured with a BioRad ChemiDoc. (B) Surface area coverage of the plate was determined using FIJI (ImageJ) software. Swarming was significantly reduced in CF isolates compared to strain PAO1. The mean is displayed as a horizontal line. Significant differences (**** $P < 0.0001$) between CF isolates and the strain PAO1 were determined by ANOVA followed by Dunnett's post-hoc analysis. (C) Pyocyanin was extracted from the supernatants of overnight cultures and measured using a spectrophotometer ($\text{OD}_{520\text{nm}}$). LESB58, which is known to overproduce pyocyanin [71], exhibited significantly increased pyocyanin production relative to PAO1 and CF clinical isolates. The mean is displayed as a horizontal line. Significant differences (* $P < 0.05$, **** $P < 0.0001$) between CF isolates and the strain PAO1 were determined by ANOVA followed by Dunnett's post-hoc analysis.

(PPTX)

S9 Fig. Colistin had reduced efficacy on persistent RP73 strain in infected zebrafish.

Embryos colonized for 1.5 or 48 h were subjected to colistin challenge (10 $\mu\text{g}/\text{ml}$), or incubated in water for the control condition ($n = 2$ to 3, 10 to 15 larvae). Following 30 min antibiotic treatment, bacterial load per embryo was determined in both groups. Mann-Whitney test: **** $P < 0.0001$. Ratios were calculated regarding the median of the data set.

(PPTX)

S10 Fig. Isolate B6513 responds to hANP *in vitro*. (A) *In vitro* biofilms formed by the isolate B6513 for 24 h at 37 $^{\circ}\text{C}$ in dynamic conditions were either untreated (left) or exposed to hANP at 0.1 μM (right) for 2 h, and were imaged by confocal microscopy following SYTO9 staining of bacterial cells. (B) COMSTAT analysis of biofilms imaged in (A), six views were extracted from two independent biological experiments ($n = 2$). Student's t-test: **** $P < 0.0001$.

(PPTX)

S11 Fig. Complete kinetic of the effect of anti-biofilm compounds. Effect of hANP, CDA and H_2O (control) shown in Fig 6, with a shorter time frame between images (0.5 h compared to 2.5 h). Scale bar: 40 μm .

(PPTX)

S1 Table. Detailed program of microwave processing used for resin embedding.

(DOCX)

Acknowledgments

We thank M. Bour and K. Jeannot (French National Reference Centre for antimicrobial resistance, Besançon, France) for providing and sequencing the clinical strains A6520, B6513 and C6490, and A. Bragonzi (Milano, Italy) for providing the strain RP73. We thank the imaging facility MRI, member of the national infrastructure France-BioImaging infrastructure supported by the French National Research Agency (ANR-10-INBS-04, «Investments for the future») for photonic microscopy at the MRI-DBS-UM platform and training by V. Diakou and E. Jublanc. We thank C. Gonzalez and V. Goulian for the Aquatic model facility ZEFIX from LPHI. Aquatic facility is supported by European Community's H2020 Program

[Marie-Curie Innovative Training Network Inflanet: Grant Agreement n° 955576]. We thank G. Lutfalla (LPHI, Montpellier, France) and P. Huber (Université Grenoble Alpes, CEA, France) for critical reading of the manuscript.

Author contributions

Conceptualization: Stéphane Pont, Flore Nilly, Anne-Béatrice Blanc-Potard.

Formal analysis: Stéphane Pont, Flore Nilly.

Funding acquisition: Robert EW Hancock, Anne-Béatrice Blanc-Potard.

Investigation: Stéphane Pont, Flore Nilly, Laurence Berry, Anne Bonhoure, Morgan A Alford, Mélissande Louis, Pauline Nogaret, Manjeet Bains.

Methodology: Stéphane Pont, Flore Nilly, Laurence Berry, Anne Bonhoure, Anne-Béatrice Blanc-Potard.

Project administration: Anne-Béatrice Blanc-Potard.

Resources: Patrick Plésiat.

Supervision: Robert EW Hancock, Anne-Béatrice Blanc-Potard.

Validation: Stéphane Pont, Flore Nilly, Anne Bonhoure, Morgan A Alford, Anne-Béatrice Blanc-Potard.

Visualization: Stéphane Pont, Flore Nilly, Laurence Berry, Anne Bonhoure, Morgan A Alford, Mélissande Louis.

Writing – original draft: Stéphane Pont, Anne-Béatrice Blanc-Potard.

Writing – review & editing: Stéphane Pont, Olivier Lesouhaitier, Robert EW Hancock, Patrick Plésiat, Anne-Béatrice Blanc-Potard.

References

1. Qin SG, Xiao W, Zhou CM, Pu QQ, Deng X, Lan LF, et al. *Pseudomonas aeruginosa*: pathogenesis, virulence factors, antibiotic resistance, interaction with host, technology advances and emerging therapeutics. *Signal Transduct Tar*. 2022. <https://doi.org/10.1038%2Fs41392-022-01056-1>
2. Garcia-Clemente M, de la Rosa D, Máiz L, Girón R, Blanco M, Oliveira C, et al. Impact of *Pseudomonas aeruginosa* Infection on patients with chronic inflammatory airway diseases. *J Clin Med*. 2020;9(12):3800. <https://doi.org/10.3390/jcm9123800> PMID: [33255354](https://pubmed.ncbi.nlm.nih.gov/33255354/)
3. Serra R, Grande R, Butrico L, Rossi A, Settimio UF, Caroleo B, et al. Chronic wound infections: the role of *Pseudomonas aeruginosa* and *Staphylococcus aureus*. *Expert Rev Anti Infect Ther*. 2015;13(5):605–13. <https://doi.org/10.1586/14787210.2015.1023291> PMID: [25746414](https://pubmed.ncbi.nlm.nih.gov/25746414/)
4. Moradali MF, Ghods S, Rehm BHA. *Pseudomonas aeruginosa* lifestyle: a paradigm for adaptation, survival, and persistence. *Front Cell Infect Microbiol*. 2017;7:39. <https://doi.org/10.3389/fcimb.2017.00039> PMID: [28261568](https://pubmed.ncbi.nlm.nih.gov/28261568/)
5. Tacconelli E, Carrara E, Savoldi A, Harbarth S, Mendelson M, Monnet DL, et al. Discovery, research, and development of new antibiotics: the WHO priority list of antibiotic-resistant bacteria and tuberculosis. *Lancet Infect Dis*. 2018;18(3):318–27. [https://doi.org/10.1016/S1473-3099\(17\)30753-3](https://doi.org/10.1016/S1473-3099(17)30753-3) PMID: [29276051](https://pubmed.ncbi.nlm.nih.gov/29276051/)
6. Brauner A, Fridman O, Gefen O, Balaban NQ. Distinguishing between resistance, tolerance and persistence to antibiotic treatment. *Nat Rev Microbiol*. 2016;14(5):320–30. <https://doi.org/10.1038/nrmi-cro.2016.34> PMID: [27080241](https://pubmed.ncbi.nlm.nih.gov/27080241/)
7. La Rosa R, Johansen HK, Molin S. Persistent bacterial infections, antibiotic treatment failure, and microbial adaptive evolution. *Antibiotics (Basel)*. 2022;11(3):419. <https://doi.org/10.3390/antibiotics11030419> PMID: [35326882](https://pubmed.ncbi.nlm.nih.gov/35326882/)
8. Kember M, Grandy S, Raudonis R, Cheng Z. Non-canonical host intracellular niche links to new antimicrobial resistance mechanism. *Pathogens*. 2022;11(2):220. <https://doi.org/10.3390/pathogens11020220> PMID: [35215166](https://pubmed.ncbi.nlm.nih.gov/35215166/)

9. Resko ZJ, Suhi RF, Thota AV, Kroken AR. Evidence for intracellular *Pseudomonas aeruginosa*. *J Bacteriol.* 2024;206(5):e0010924. <https://doi.org/10.1128/jb.00109-24> PMID: [38597609](https://pubmed.ncbi.nlm.nih.gov/38597609/)
10. Malet K, Faure E, Adam D, Donner J, Liu L, Pilon S-J, et al. Intracellular *Pseudomonas aeruginosa* within the airway epithelium of cystic fibrosis lung tissues. *Am J Respir Crit Care Med.* 2024;209(12):1453–62. <https://doi.org/10.1164/rccm.202308-1451OC> PMID: [38324627](https://pubmed.ncbi.nlm.nih.gov/38324627/)
11. Buyck JM, Tulkens PM, Van Bambeke F. Pharmacodynamic evaluation of the intracellular activity of antibiotics towards *Pseudomonas aeruginosa* PAO1 in a model of THP-1 human monocytes. *Antimicrob Agents Chemother.* 2013;57(5):2310–8. <https://doi.org/10.1128/AAC.02609-12> PMID: [23478951](https://pubmed.ncbi.nlm.nih.gov/23478951/)
12. Garcia-Medina R, Dunne WM, Singh PK, Brody SL. *Pseudomonas aeruginosa* acquires biofilm-like properties within airway epithelial cells. *Infect Immun.* 2005;73(12):8298–305. <https://doi.org/10.1128/IAI.73.12.8298-8305.2005> PMID: [16299327](https://pubmed.ncbi.nlm.nih.gov/16299327/)
13. Penaranda C, Chumbler NM, Hung DT. Dual transcriptional analysis reveals adaptation of host and pathogen to intracellular survival of *Pseudomonas aeruginosa* associated with urinary tract infection. *PLoS Pathog.* 2021;17(4):e1009534. <https://doi.org/10.1371/journal.ppat.1009534> PMID: [33901267](https://pubmed.ncbi.nlm.nih.gov/33901267/)
14. Lorenz A, Pawar V, Häussler S, Weiss S. Insights into host-pathogen interactions from state-of-the-art animal models of respiratory *Pseudomonas aeruginosa* infections. *FEBS Lett.* 2016;590(21):3941–59. <https://doi.org/10.1002/1873-3468.12454> PMID: [27730639](https://pubmed.ncbi.nlm.nih.gov/27730639/)
15. Reyne N, McCarron A, Cmielewski P, Parsons D, Donnelley M. To bead or not to bead: A review of *Pseudomonas aeruginosa* lung infection models for cystic fibrosis. *Front Physiol.* 2023;14:1104856. <https://doi.org/10.3389/fphys.2023.1104856> PMID: [36824474](https://pubmed.ncbi.nlm.nih.gov/36824474/)
16. Pletzer D, Mansour SC, Wuert K, Rahanjam N, Hancock REW. New mouse model for chronic infections by gram-negative bacteria enabling the study of anti-infective efficacy and host-microbe interactions. *mBio.* 2017;8(1):e00140–17. <https://doi.org/10.1128/mBio.00140-17> PMID: [28246361](https://pubmed.ncbi.nlm.nih.gov/28246361/)
17. Meeker ND, Trede NS. Immunology and zebrafish: spawning new models of human disease. *Dev Comp Immunol.* 2008;32(7):745–57. <https://doi.org/10.1016/j.dci.2007.11.011> PMID: [18222541](https://pubmed.ncbi.nlm.nih.gov/18222541/)
18. Pont S, Blanc-Potard A-B. Zebrafish embryo infection model to investigate *pseudomonas aeruginosa* interaction with innate immunity and validate new therapeutics. *Front Cell Infect Microbiol.* 2021;11:745851. <https://doi.org/10.3389/fcimb.2021.745851> PMID: [34660345](https://pubmed.ncbi.nlm.nih.gov/34660345/)
19. Torraca V, Mostowy S. Zebrafish infection: from pathogenesis to cell biology. *Trends Cell Biol.* 2018;28(2):143–56. <https://doi.org/10.1016/j.tcb.2017.10.002> PMID: [29173800](https://pubmed.ncbi.nlm.nih.gov/29173800/)
20. Moussouni M, Berry L, Sipka T, Nguyen-Chi M, Blanc-Potard A-B. *Pseudomonas aeruginosa* OprF plays a role in resistance to macrophage clearance during acute infection. *Sci Rep.* 2021;11(1):359. <https://doi.org/10.1038/s41598-020-79678-0> PMID: [33432030](https://pubmed.ncbi.nlm.nih.gov/33432030/)
21. Phennicie RT, Sullivan MJ, Singer JT, Yoder JA, Kim CH. Specific resistance to *Pseudomonas aeruginosa* infection in zebrafish is mediated by the cystic fibrosis transmembrane conductance regulator. *Infect Immun.* 2010;78(11):4542–50. <https://doi.org/10.1128/IAI.00302-10> PMID: [20732993](https://pubmed.ncbi.nlm.nih.gov/20732993/)
22. Kumar SS, Tandberg JI, Penesyan A, Elbourne LDH, Suarez-Bosche N, Don E, et al. Dual Transcriptomics of host-pathogen interaction of cystic fibrosis Isolate *Pseudomonas aeruginosa* PASS1 With Zebrafish. *Front Cell Infect Microbiol.* 2018;8:406. <https://doi.org/10.3389/fcimb.2018.00406> PMID: [30524971](https://pubmed.ncbi.nlm.nih.gov/30524971/)
23. Nogaret P, El Garah F, Blanc-Potard A-B. A novel infection protocol in Zebrafish embryo to assess *Pseudomonas aeruginosa* virulence and validate efficacy of a quorum sensing inhibitor *In Vivo*. *Pathogens.* 2021;10(4):401. <https://doi.org/10.3390/pathogens10040401> PMID: [33805384](https://pubmed.ncbi.nlm.nih.gov/33805384/)
24. Hajjar H, Berry L, Wu Y, Touqui L, Vergunst AC, Blanc-Potard A-B. Contribution of intramacrophage stages to *Pseudomonas aeruginosa* infection outcome in zebrafish embryos: insights from *mgfC* and *oprF* mutants. *Sci Rep.* 2024;14(1):6297. <https://doi.org/10.1038/s41598-024-56725-8> PMID: [38491095](https://pubmed.ncbi.nlm.nih.gov/38491095/)
25. Facchini M, De Fino I, Riva C, Bragonzi A. Long term chronic *Pseudomonas aeruginosa* airway infection in mice. *J Vis Exp.* 2014;(85):51019. <https://doi.org/10.3791/51019> PMID: [24686327](https://pubmed.ncbi.nlm.nih.gov/24686327/)
26. Bianconi I, Jeukens J, Freschi L, Alcalá-Franco B, Facchini M, Boyle B, et al. Comparative genomics and biological characterization of sequential *Pseudomonas aeruginosa* isolates from persistent airways infection. *BMC Genomics.* 2015;16:1105. <https://doi.org/10.1186/s12864-015-2276-8> PMID: [26714629](https://pubmed.ncbi.nlm.nih.gov/26714629/)
27. Sousa AM, Pereira MO. *Pseudomonas aeruginosa* diversification during infection development in cystic fibrosis lungs—a review. *Pathogens.* 2014;3(3):680–703. <https://doi.org/10.3390/pathogens3030680> PMID: [25438018](https://pubmed.ncbi.nlm.nih.gov/25438018/)
28. Brannon MK, Davis JM, Mathias JR, Hall CJ, Emerson JC, Crosier PS, et al. *Pseudomonas aeruginosa* Type III secretion system interacts with phagocytes to modulate systemic infection of zebrafish

- embryos. *Cell Microbiol.* 2009;11(5):755–68. <https://doi.org/10.1111/j.1462-5822.2009.01288.x> PMID: [19207728](https://pubmed.ncbi.nlm.nih.gov/19207728/)
29. Clatworthy AE, Lee JS-W, Leibman M, Kostun Z, Davidson AJ, Hung DT. *Pseudomonas aeruginosa* infection of zebrafish involves both host and pathogen determinants. *Infect Immun.* 2009;77(4):1293–303. <https://doi.org/10.1128/IAI.01181-08> PMID: [19168742](https://pubmed.ncbi.nlm.nih.gov/19168742/)
 30. Cafora M, Deflorian G, Forti F, Ferrari L, Binelli G, Briani F, et al. Phage therapy against *Pseudomonas aeruginosa* infections in a cystic fibrosis zebrafish model. *Sci Rep.* 2019;9(1):1527. <https://doi.org/10.1038/s41598-018-37636-x> PMID: [30728389](https://pubmed.ncbi.nlm.nih.gov/30728389/)
 31. Mittal R, Grati M, Gerring R, Blackwelder P, Yan D, Li J-D, et al. In vitro interaction of *Pseudomonas aeruginosa* with human middle ear epithelial cells. *PLoS One.* 2014;9(3):e91885. <https://doi.org/10.1371/journal.pone.0091885> PMID: [24632826](https://pubmed.ncbi.nlm.nih.gov/24632826/)
 32. Angus AA, Lee AA, Augustin DK, Lee EJ, Evans DJ, Fleiszig SMJ. *Pseudomonas aeruginosa* induces membrane blebs in epithelial cells, which are utilized as a niche for intracellular replication and motility. *Infect Immun.* 2008;76(5):1992–2001. <https://doi.org/10.1128/IAI.01221-07> PMID: [18316391](https://pubmed.ncbi.nlm.nih.gov/18316391/)
 33. Fleiszig SM, Zaidi TS, Fletcher EL, Preston MJ, Pier GB. *Pseudomonas aeruginosa* invades corneal epithelial cells during experimental infection. *Infect Immun.* 1994;62(8):3485–93. <https://doi.org/10.1128/iai.62.8.3485-3493.1994> PMID: [8039920](https://pubmed.ncbi.nlm.nih.gov/8039920/)
 34. Garai P, Berry L, Mousouni M, Bleves S, Blanc-Potard A-B. Killing from the inside: Intracellular role of T3SS in the fate of *Pseudomonas aeruginosa* within macrophages revealed by mgtC and oprF mutants. *PLoS Pathog.* 2019;15(6):e1007812. <https://doi.org/10.1371/journal.ppat.1007812> PMID: [31220187](https://pubmed.ncbi.nlm.nih.gov/31220187/)
 35. Belon C, Soscia C, Bernut A, Laubier A, Bleves S, Blanc-Potard A-B. A macrophage subversion factor is shared by intracellular and extracellular pathogens. *PLoS Pathog.* 2015;11(6):e1004969. <https://doi.org/10.1371/journal.ppat.1004969> PMID: [26080006](https://pubmed.ncbi.nlm.nih.gov/26080006/)
 36. Weimann A, Dinan AM, Ruis C, Bernut A, Pont S, Brown K, et al. Evolution and host-specific adaptation of *Pseudomonas aeruginosa*. *Science.* 2024;385(6704):ead0908. <https://doi.org/10.1126/science.ad0908> PMID: [38963857](https://pubmed.ncbi.nlm.nih.gov/38963857/)
 37. Papadimitriou-Olivgeris M, Jacot D, Guery B. How to manage *Pseudomonas aeruginosa* infections. *Adv Exp Med Biol.* 2022;1386:425–45. https://doi.org/10.1007/978-3-031-08491-1_16 PMID: [36258082](https://pubmed.ncbi.nlm.nih.gov/36258082/)
 38. Volpe DA. Permeability classification of representative fluoroquinolones by a cell culture method. *AAPS J.* 2004;6(2):1–6. <https://doi.org/10.1208/ps060213> PMID: [18465265](https://pubmed.ncbi.nlm.nih.gov/18465265/)
 39. Louis M, Clamens T, Tahrioui A, Desriac F, Rodrigues S, Rosay T, et al. *Pseudomonas aeruginosa* biofilm dispersion by the human atrial natriuretic peptide. *Adv Sci (Weinh).* 2022;9(7):e2103262. <https://doi.org/10.1002/advs.202103262> PMID: [35032112](https://pubmed.ncbi.nlm.nih.gov/35032112/)
 40. Rahmani-Badi A, Sepehr S, Fallahi H, Heidari-Kesher S. Dissection of the *cis*-2-decenoic acid signaling network in using microarray technique. *Frontiers in microbiology.* 2015. <https://doi.org/10.3389/fmicb.2015.00383>
 41. Sepehr S, Rahmani-Badi A, Babaie-Naiej H, Soudi MR. Unsaturated fatty acid, *cis*-2-decenoic acid, in combination with disinfectants or antibiotics removes pre-established biofilms formed by food-related bacteria. *PLoS One.* 2014;9(7):e101677. <https://doi.org/10.1371/journal.pone.0101677> PMID: [25000301](https://pubmed.ncbi.nlm.nih.gov/25000301/)
 42. Prudent V, Demarre G, Vazeille E, Wery M, Quenech'Du N, Ravet A, et al. The Crohn's disease-related bacterial strain LF82 assembles biofilm-like communities to protect itself from phagolysosomal attack. *Commun Biol.* 2021;4(1):627. <https://doi.org/10.1038/s42003-021-02161-7> PMID: [34035436](https://pubmed.ncbi.nlm.nih.gov/34035436/)
 43. Torraca V, Brokatzky D, Miles SL, Chong CE, De Silva PM, Baker S, et al. *Shigella* serotypes associated with carriage in humans establish persistent infection in Zebrafish. *J Infect Dis.* 2023;228(8):1108–18. <https://doi.org/10.1093/infdis/jiad326> PMID: [37556724](https://pubmed.ncbi.nlm.nih.gov/37556724/)
 44. Leiba J, Sipka T, Begon-Pescia C, Bernardello M, Tairi S, Bossi L, et al. Dynamics of macrophage polarization support *Salmonella* persistence in a whole living organism. *Elife.* 2024;13:e89828. <https://doi.org/10.7554/eLife.89828> PMID: [38224094](https://pubmed.ncbi.nlm.nih.gov/38224094/)
 45. McCarthy RR, Mazon-Moya MJ, Moscoso JA, Hao Y, Lam JS, Bordi C, et al. Cyclic-di-GMP regulates lipopolysaccharide modification and contributes to *Pseudomonas aeruginosa* immune evasion. *Nat Microbiol.* 2017;2:17027. <https://doi.org/10.1038/nmicrobiol.2017.27> PMID: [28263305](https://pubmed.ncbi.nlm.nih.gov/28263305/)
 46. Kumar NG, Nieto V, Kroken AR, Jedel E, Grosser MR, Hallsten ME, et al. *Pseudomonas aeruginosa* can diversify after host cell invasion to establish multiple intracellular niches. *mBio.* 2022;13(6):e0274222. <https://doi.org/10.1128/mbio.02742-22> PMID: [36374039](https://pubmed.ncbi.nlm.nih.gov/36374039/)

47. Newman JN, Floyd RV, Fothergill JL. Invasion and diversity in *Pseudomonas aeruginosa* urinary tract infections. *J Med Microbiol.* 2022;71(3):001458. <https://doi.org/10.1099/jmm.0.001458> PMID: [35275806](https://pubmed.ncbi.nlm.nih.gov/35275806/)
48. Del Mar Cendra M, Torrents E. Differential adaptability between reference strains and clinical isolates of *Pseudomonas aeruginosa* into the lung epithelium intracellular lifestyle. *Virulence.* 2020;11(1):862–76. <https://doi.org/10.1080/21505594.2020.1787034> PMID: [32697923](https://pubmed.ncbi.nlm.nih.gov/32697923/)
49. Malet JK, Hennemann LC, Hua EM-L, Faure E, Waters V, Rousseau S, et al. A model of intracellular persistence of *Pseudomonas aeruginosa* in airway epithelial cells. *Cellular Microbio.* 2022;2022:1–14. <https://doi.org/10.1155/2022/5431666>
50. Bjarnsholt T, Alhede M, Alhede M, Eickhardt-Sørensen SR, Moser C, Kühl M, et al. The in vivo biofilm. *Trends Microbiol.* 2013;21(9):466–74. <https://doi.org/10.1016/j.tim.2013.06.002> PMID: [23827084](https://pubmed.ncbi.nlm.nih.gov/23827084/)
51. Lichtenberg M, Kirketerp-Møller K, Kvich LA, Christensen MH, Fritz B, Jakobsen TH, et al. Single cells and bacterial biofilm populations in chronic wound infections. *APMIS.* 2024;132(12):1071–7. <https://doi.org/10.1111/apm.13344> PMID: [37718461](https://pubmed.ncbi.nlm.nih.gov/37718461/)
52. Kragh KN, Tolker-Nielsen T, Lichtenberg M. The non-attached biofilm aggregate. *Commun Biol.* 2023;6(1):898. <https://doi.org/10.1038/s42003-023-05281-4> PMID: [37658117](https://pubmed.ncbi.nlm.nih.gov/37658117/)
53. Pang Z, Raudonis R, Glick BR, Lin T-J, Cheng Z. Antibiotic resistance in *Pseudomonas aeruginosa*: mechanisms and alternative therapeutic strategies. *Biotechnol Adv.* 2019;37(1):177–92. <https://doi.org/10.1016/j.biotechadv.2018.11.013> PMID: [30500353](https://pubmed.ncbi.nlm.nih.gov/30500353/)
54. Lamberti Y, Surmann K. The intracellular phase of extracellular respiratory tract bacterial pathogens and its role on pathogen-host interactions during infection. *Curr Opin Infect Dis.* 2021;34(3):197–205. <https://doi.org/10.1097/QCO.0000000000000727> PMID: [33899754](https://pubmed.ncbi.nlm.nih.gov/33899754/)
55. Mirzaei R, Mohammadzadeh R, Sholeh M, Karampoor S, Abdi M, Dogan E, et al. The importance of intracellular bacterial biofilm in infectious diseases. *Microb Pathog.* 2020;147:104393. <https://doi.org/10.1016/j.micpath.2020.104393> PMID: [32711113](https://pubmed.ncbi.nlm.nih.gov/32711113/)
56. Sycz G, Di Venanzio G, Distel JS, Sartorio MG, Le N-H, Scott NE, et al. Modern *Acinetobacter baumannii* clinical isolates replicate inside spacious vacuoles and egress from macrophages. *PLoS Pathog.* 2021;17(8):e1009802. <https://doi.org/10.1371/journal.ppat.1009802> PMID: [34370792](https://pubmed.ncbi.nlm.nih.gov/34370792/)
57. Ercoli G, Fernandes VE, Chung WY, Wanford JJ, Thomson S, Bayliss CD, et al. Intracellular replication of *Streptococcus pneumoniae* inside splenic macrophages serves as a reservoir for septicemia. *Nat Microbiol.* 2018;3(5):600–10. <https://doi.org/10.1038/s41564-018-0147-1> PMID: [29662129](https://pubmed.ncbi.nlm.nih.gov/29662129/)
58. Holloway BW. Genetic recombination in *Pseudomonas aeruginosa*. *J Gen Microbiol.* 1955;13(3):572–81. <https://doi.org/10.1099/00221287-13-3-572> PMID: [13278508](https://pubmed.ncbi.nlm.nih.gov/13278508/)
59. Pont S, Fraikin N, Caspar Y, Van Melderen L, Attrée I, Cretin F. Bacterial behavior in human blood reveals complement evaders with some persister-like features. *PLoS Pathog.* 2020;16(12):e1008893. <https://doi.org/10.1371/journal.ppat.1008893> PMID: [33326490](https://pubmed.ncbi.nlm.nih.gov/33326490/)
60. Phan QT, Sipka T, Gonzalez C, Levraud J-P, Lutfalla G, Nguyen-Chi M. Neutrophils use superoxide to control bacterial infection at a distance. *PLoS Pathog.* 2018;14(7):e1007157. <https://doi.org/10.1371/journal.ppat.1007157> PMID: [30016370](https://pubmed.ncbi.nlm.nih.gov/30016370/)
61. Hall C, Flores MV, Storm T, Crosier K, Crosier P. The zebrafish lysozyme C promoter drives myeloid-specific expression in transgenic fish. *BMC Dev Biol.* 2007;7:42. <https://doi.org/10.1186/1471-213X-7-42> PMID: [17477879](https://pubmed.ncbi.nlm.nih.gov/17477879/)
62. Ellis K, Bagwell J, Bagnat M. Notochord vacuoles are lysosome-related organelles that function in axis and spine morphogenesis. *J Cell Biol.* 2013;200(5):667–79. <https://doi.org/10.1083/jcb.201212095> PMID: [23460678](https://pubmed.ncbi.nlm.nih.gov/23460678/)
63. Nguyen-Chi M, Luz-Crawford P, Balas L, Sipka T, Contreras-López R, Barthelaix A, et al. Pro-resolving mediator protectin D1 promotes epimorphic regeneration by controlling immune cell function in vertebrates. *Br J Pharmacol.* 2020;177(17):4055–73. <https://doi.org/10.1111/bph.15156> PMID: [32520398](https://pubmed.ncbi.nlm.nih.gov/32520398/)
64. Begon-Pescia C, Boireau S, Boyer-Clavel M, Lutfalla G, Nguyen-Chi M. Preparing sequencing grade RNAs from a small number of FACS-sorted larvae macrophages isolated from enzyme free dissociated zebrafish larvae. *MethodsX.* 2022;9:101651. <https://doi.org/10.1016/j.mex.2022.101651> PMID: [35342722](https://pubmed.ncbi.nlm.nih.gov/35342722/)
65. Kimmel CB, Ballard WW, Kimmel SR, Ullmann B, Schilling TF. Stages of embryonic development of the zebrafish. *Dev Dyn.* 1995;203(3):253–310. <https://doi.org/10.1002/aja.1002030302> PMID: [8589427](https://pubmed.ncbi.nlm.nih.gov/8589427/)
66. Hua Y, Laserstein P, Helmstaedter M. Large-volume en-bloc staining for electron microscopy-based connectomics. *Nat Commun.* 2015;6:7923. <https://doi.org/10.1038/ncomms8923> PMID: [26235643](https://pubmed.ncbi.nlm.nih.gov/26235643/)

67. Moussouni M, Nogaret P, Garai P, Ize B, Vivès E, Blanc-Potard A-B. Activity of a synthetic peptide targeting MgtC on *Pseudomonas aeruginosa* intramacrophage survival and biofilm formation. *Front Cell Infect Microbiol.* 2019;9:84. <https://doi.org/10.3389/fcimb.2019.00084> PMID: [31001488](https://pubmed.ncbi.nlm.nih.gov/31001488/)
68. Essar DW, Eberly L, Hadero A, Crawford IP. Identification and characterization of genes for a second anthranilate synthase in *Pseudomonas aeruginosa*: interchangeability of the two anthranilate synthases and evolutionary implications. *J Bacteriol.* 1990;172(2):884–900. <https://doi.org/10.1128/jb.172.2.884-900.1990> PMID: [2153661](https://pubmed.ncbi.nlm.nih.gov/2153661/)
69. Tolker-Nielsen T, Sternberg C. Growing and analyzing biofilms in flow chambers. *Curr Protoc Microbiol.* 2011;Chapter 1:Unit 1B.2. <https://doi.org/10.1002/9780471729259.mc01b02s21> PMID: [21538301](https://pubmed.ncbi.nlm.nih.gov/21538301/)
70. Heydorn A, Nielsen AT, Hentzer M, Sternberg C, Givskov M, Ersbøll BK, et al. Quantification of biofilm structures by the novel computer program COMSTAT. *Microbiology (Reading).* 2000;146 (Pt 10):2395–407. <https://doi.org/10.1099/00221287-146-10-2395> PMID: [11021916](https://pubmed.ncbi.nlm.nih.gov/11021916/)
71. Fothergill JL, Panagea S, Hart CA, Walshaw MJ, Pitt TL, Winstanley C. Widespread pyocyanin over-production among isolates of a cystic fibrosis epidemic strain. *BMC Microbiol.* 2007;7:45. <https://doi.org/10.1186/1471-2180-7-45> PMID: [17521417](https://pubmed.ncbi.nlm.nih.gov/17521417/)